Solution of the multichannel Coqblin-Schrieffer impurity model and application to multilevel systems

Andrés Jerez*
Department of Physics, Theoretical Physics, University of Oxford, 1 Keble Road, Oxford OX1 3NP, United Kingdom

Natan Andrei
Department of Physics and Astronomy, Rutgers University, Piscataway, New Jersey 08855

Gergely Zaránd
Institute of Physics, Technical University of Budapest, H 1521 Budafoki út 8., Budapest, Hungary
(Received 27 February 1998)

A complete Bethe ansatz solution of the SU(N)×SU(f) Coqblin-Schrieffer model and a detailed analysis of some physical applications of the model are given. As in the usual multichannel Kondo model, a variety of Fermi-liquid and non-Fermi-liquid (NFL) fixed points is found, whose nature depends on the impurity representation μ. For $\mu=f$, we find a Fermi-liquid fixed point, with the impurity spin completely screened. For $f>\mu$, the impurity is overscreened and the model has NFL properties. The form the NFL behavior takes depends on the N and f: for $N\leqslant f$, the specific heat and the susceptibility are dominated by the NFL contributions; for $N>f$ the leading contributions are Fermi-liquid-like, and the NFL behavior can be seen only to subleading order; and for $N=f$ the behavior is marginal. We also analyze the possibility of physical realizations. We show by a detailed renormalization-group and $1/f$ analysis that the tunneling N-state problem can be mapped into the SU(N)×SU(f) exchange model, and discuss the subtle differences between the two models. As another physical realization we suggest a double quantum dot structure that can be described by means of an SU(3)×SU(2) model if the parameters of the dots are tuned appropriately. [S0163-1829(98)01528-8]

I. INTRODUCTION

The multichannel Kondo model[1] is the simplest impurity model with non-Fermi-liquid behavior. Originally introduced to describe ''real metals'' with magnetic impurities, its applications go beyond the study of dilute magnetic alloys. For instance, it has been known for some time that systems consisting of heavy atoms tunneling between two neighboring sites and interacting with conduction electrons are a realization of the two-channel Kondo model.[2] Another realization is the quadrupolar Kondo effect in the context of heavy fermions.[3] A detailed account of various aspects and applications of the multichannel Kondo model is given in Ref. 4.

For materials such as $Pb_{1-x}Ge_xTe$ or $K_{1-x}Li_xCl$ alloys, tunneling may occur between an arbitrary number of levels. Such systems could be modeled using a multichannel version of the Coqblin-Schrieffer model, a SU(N)×SU(f) Kondo model.[5] Here N is the number of spin degrees of freedom, and f is the number of channels, or $flavor$ degrees of freedom.

In this paper we present an exact solution of the SU(N)×SU(f) Kondo model, and study the thermodynamic properties of the system. We obtain the leading exponents for the impurity contribution to the magnetic susceptibility and specific heat for arbitrary N and f. We also discuss the effects of channel anisotropy, which might drive the system from a fixed point with $\gamma\equiv f/N>1$ to a new fixed point where $\gamma^{eff}<1$.

II. THE MODEL

The multichannel Coqblin-Schrieffer model describes electrons carrying two sets of internal degrees of freedom, to be denoted spin and flavor (or channel number), interacting with an impurity carrying only spin. The impurity is localized at a point chosen to be the origin. The Hamiltonian reads

$$\mathcal{H}=-i\sum_{a}^{N}\sum_{m}^{f}\int_{-\infty}^{\infty}\psi_{a,m}^{\dagger}(x)\partial_x\psi_{a,m}(x)dx + 2\sum_{m}^{f}J_m\sum_{\alpha}^{N^2-1}\sum_{a,b}^{N}\psi_{a,m}^{\dagger}(0)(T_{\alpha}^{(\square)})_{a,b}\psi_{b,m}(0) \times\sum_{a',b'}^{dim(\mu)}\chi_{a'}^{\dagger}(T_{\alpha}^{(\mu)})_{a',b'}\chi_{b'}. \quad (2.1)$$

Both $\psi_{a,m}^{\dagger}(x)$ and $\chi_a^{\dagger}$ are fermionic fields; the former creates an electron at x with spin index a and flavor index m, while the latter creates the impurity at $x=0$. Imposing the condition $\Sigma_a\chi_a^{\dagger}\chi_a=1$, we have that $\chi_{a'}^{\dagger}(T_{\alpha}^{(\mu)})_{a',b'}\chi_{b'}$ represents the impurity spin operator in a representation of SU(N) specified by a particular choice of the matrices $T_{\alpha}^{(rep)}$, where the index α runs from 1 to N^2-1, the number of generators of SU(N). We will restrict ourselves to the case in which the electrons are in the fundamental representation [denoted by ($\square$)], and the impurity is in the totally symmetric representation obtained from the direct product of μ fundamental representations.

The physical realizations discussed in the present paper correspond to the simplest case, $\mu=1$; the investigation of the $\mu>1$ cases gives us important insight into the general structure of the model, and allows, in particular, for a com-

parison with the results obtained for the multichannel Kondo model with impurity spin $S>\frac{1}{2}$.

In most of this paper we will study the isotropic model, $J_m=J$, with the symmetry $U(1)^{charge}\times \mathrm{SU}(N)^{spin}\times \mathrm{SU}(f)^{flavor}$. We will also assume that the different flavor levels are equally populated, $N^e=fN_0$.

In what follows shall solve the complete model and, among other things, study its low-energy physics. As is well known, the low-energy behavior of a system can often be described in terms of effective Hamiltonians, that are simpler than the starting Hamiltonian; these are usually referred to as fixed points. We shall determine their properties from the exact solution. We shall find that the model possesses a variety of fixed points (or low-energy regimes), whose nature depends on the symmetry structure in the flavor sector and on the spin representation (μ), generalizing the familiar $N=2$ case (the multichannel Kondo model[1]). As previously, we shall identify the mechanism underlying the appearance of these fixed points as *dynamical fusion* by which electrons form spin complexes whose interaction with the impurity leads to an interesting behavior in the infrared.[6] Each complex consists of f electrons fused into a local objects that transforms according to one-row Young tableaux of length f.

Within the Bethe ansatz approach, a precise description of the formation of these composites can be given. The linearized Hamiltonian separately propagates the charge-spin-flavor degrees of freedom that make up the electron. Therefore, the effect of flavor on the spin degrees of freedom is recovered only in the physical space. To follow the dynamic coupling of spin and flavor, we add some curvature, which maintains the identity of the electron while allowing its components to interact. It has the form $H_\Lambda=(1/2\Lambda)\,\Sigma_a\Sigma_m\int_{-\infty}^{\infty}\psi^\dagger_{a,m}(x)\partial_x^2\psi_{a,m}(x)dx$, where Λ is the curvature scale which is sent to infinity at the end of the calculation. Adding this term allows for the formation of bound states in the flavor singlet channel, which interact strongly with the impurity, and determine the low-energy dynamics even after the curvature is removed. A close analogy is a small magnetic field introduced to probe for magnetization, which may survive after the field is removed. Imposing a cutoff D on the momentum variables guarantees the finiteness of the energy. Other terms need to be added to the Hamiltonian to maintain integrability, terms which we shall see below are irrelevant.

For free fields, the resulting theory is already quite involved, and even the counting of states is not trivial.[7] Nevertheless, the charge-spin-flavor separated basis is the natural one for the noninteracting problem, as we shall see later: it is the form to which the eigenstates tend when the interaction is turned off. We thus introduce the following elements.

(i) A second derivative term with a curvature scale, Λ,

$$H_\Lambda=\frac{1}{2\Lambda}\sum_a\sum_m\int_{-\infty}^{\infty}\psi^\dagger_{a,m}(x)\partial_x^2\psi_{a,m}(x)dx, \tag{2.2}$$

which breaks charge-spin-flavor separation of the linear spectrum. Once the electron composites are formed, and the low-energy spectrum of the theory is identified, the scale is taken to infinity. Adding the term (2.2) also imposes restrictions on the form of the eigenstates which can be expressed in terms of the following counterterms without which the model is not integrable for finite Λ.

(ii) An electron-electron interaction term of the form

$$2\tilde{J}\sum_{m,m'}\sum_{a,a'}\int_{-\infty}^{\infty}\psi^\dagger_{a,m}(x)\psi^\dagger_{a',m'}(x)\psi_{a,m'}(x)\psi_{a',m}(x)dx. \tag{2.3}$$

When no impurity is present, $\tilde{J}$ can be chosen arbitrarily, since the term has no effect on the linear spectrum. The linearized spectrum has a large degeneracy, and the inclusion of Eqs. (2.2) and (2.3) will provide a way to find the eigenstates.

(iii) A counterterm H_{cc} of the form

$$H_{cc}=-\frac{1}{\Lambda}\sum_m^f\sum_a^N\int_{-\infty}^{\infty}\psi^\dagger_{a,m}(x)V(x)\psi_{a,m}(x)dx, \tag{2.4}$$

with

$$V(x)=\frac{x}{|x|}[\,\delta'(x^{+0})+\delta'(x^{-0})], \tag{2.5}$$

needs to be added to the Hamiltonian in order to preserve integrability at the origin; this term vanishes once the curvature is removed, and plays no further role in the problem.

A. First quantized Hamiltonian

A general Fock state of N^e electrons and one impurity can be written in the following form:

$$|F\rangle=\sum_{\{m_j\}}\sum_{\{a_j\},b}\int_{-\infty}^{\infty}\left(\prod_j dx_j\right)F^{\{m_j\}}_{\{a_j\},b}(\{x_j\})\times\chi^\dagger_b(0)\prod_{j=1}^{N_e}\psi^\dagger_{a_j,m_j}(x_j)|0\rangle.$$

In order for it to be an eigenstate, the amplitudes F must satisfy the equation $hF=EF$, where the differential operator h, known as the *first quantized form of the Hamiltonian*, takes the form

$$h=\sum_{j=1}^{N^e}\left\{-i\partial_j+\frac{1}{2\Lambda}\partial_j^2+2J\delta(x_j)\sum_\alpha^{N^2-1}(T^{(\Box)}_{\alpha,j})(T^{(\mu)}_\alpha)\right\}+\sum_{l<j}2\tilde{J}\delta(x_l-x_j)(P_{lj}-\mathcal{P}_{jl})-\sum_{j=1}^{N^e}\frac{1}{\Lambda}V(x_j),$$

with P_{jl} ($\mathcal{P}_{jl}$) the spin (flavor) exchange operator;

$$P_{ab,cd}=\delta_{ad}\delta_{bc},$$

$$\mathcal{P}_{m_1m_2,m_3m_4}=\delta_{m_1m_4}\delta_{m_2m_3}.$$

The fundamental representation ($\Box$) is carried by the electron j and the (μ) representation by the impurity. When the latter is also in the fundamental representation i.e., $\mu=1$, the Hamiltonian can be rewritten as

$$h=\sum_{j=1}^{N^e}\{-i\partial_j+(\Lambda^{-1})\partial_j^2+2J\delta(x_j)P_{j0}\}+\sum_{l<j}2\tilde{J}\delta(x_l-x_j)\times(P_{lj}-\mathcal{P}_{jl})+\sum_{j=1}^{N^e}\frac{1}{\Lambda}V(x_j).$$

B. *S* matrices

We will assume for now that both the electrons and the impurity are in the fundamental representation of SU(N). The eigenstate amplitudes are combinations of plane waves with *pseudomomenta* k_j, $(j=1,\ldots,N^e)$, and have coefficients that depend on the ordering of the electrons, and on the spin and the flavor indices. These coefficients are related through products of electron-impurity and electron-electron S matrices that we will derive now. Consider first the wave function describing one electron (denote it by j) interacting with the impurity (denote it by 0),

$$F^{m_j}_{a_j,a_0}(x_j)=e^{ik_jx_j}[A^{m_j}_{a_j,a_0}\theta(-x_j)+B^{m_j}_{a_j,a_0}\theta(x_j)]. \quad (2.6)$$

Applying h to it, we have (we drop the indices in the amplitudes)

$$\begin{aligned}hF(x_j)=&\left(k_j-\frac{k_j^2}{2\Lambda}\right)F(x_j)\\&\times\left[-i\left(1-\frac{k_j}{\Lambda}\right)(B-A)+JP_{j0}(B+A)\right]\delta(x_j)\\&-\frac{1}{2\Lambda}(B-A)\,\delta'(x_j)e^{ik_jx_j}+\frac{1}{\Lambda}V(x_j)F(x_j).\end{aligned} \quad (2.7)$$

F is an eigenstate of h, with eigenvalue $E_j=k_j[1-(k_j/2\Lambda)]$, if the terms in the second and third lines in Eq. (2.7) vanish. The last two terms cancel each other due to the form of Eq. (2.5). The terms in the second line of Eq. (2.7) cancel if the amplitudes A and B are related by the electron-impurity S matrix $B=S_{j0}A$, where $S_{j0}=(S_{j0})^{a_j',a_0'}_{a_j,a_0}$ is given by

$$\begin{aligned}S_{j0}=&\frac{i(1-k_j/\Lambda)+JP_{j0}}{i(1-k_j/\Lambda)-JP_{j0}}\\=&\left(\frac{i(1-k_j/\Lambda)+J}{i(1-k_j/\Lambda)-J}\right)\left(\frac{i(1-k_j/\Lambda)+JP_{j0}}{i(1-k_j/\Lambda)+J}\right)^2.\end{aligned} \quad (2.8)$$

Defining

$$c\equiv\frac{2J}{1-J^2},\quad g(x)\equiv\frac{1-x}{1-J^2}\left(1-\frac{J^2}{(1-x)^2}\right),$$

we can write

$$S_{j0}=e^{-i\,\arctan[c/g(k_j/\Lambda)]}\left(\frac{g(k_j/\Lambda)-icP_{j0}}{g(k_j/\Lambda)-ic}\right),$$

(notice that $\arctan c=2\arctan J$). Eventually we will send the cutoff to infinity. Therefore, expanding $g(k/\Lambda)$ to first order in $1/\Lambda$,

$$g(k/\Lambda)\sim 1-\left(\frac{1+J^2}{1-J^2}\right)\frac{k}{\Lambda},$$

we have

$$S_{j0}\sim e^{i\,\arctan[c/1+\lambda_j]}\left(\frac{\lambda_j-1+icP_{j0}}{\lambda_j-1+ic}\right), \quad (2.9)$$

where

$$\lambda_j=\left(\frac{1+J^2}{1-J^2}\right)\frac{k_j}{\Lambda}.$$

In the scaling limit, J and c have the same scaling behavior.

We now consider the case of two electrons. We generalize the procedure followed in the case on one electron: divide the configuration space into regions inside each of which there is no interaction, and the wave function is a superpositions of plane waves. There are six such regions in this case, corresponding to the ordering of three objects, two electrons and an impurity, and we label them by permutations $Q\in S_3$. For example, the element $Q=(1,0,2)$ labels the region where electron 1 is to the left of the impurity and electron 2 is to its right. We also introduce the notation $\theta(x_Q)$ to denote a function that takes the value 1 in the region Q, and zero elsewhere.

The two-electron wave function is then of the form (Bethe ansatz),

$$F^m_a(x)=\mathcal{A}e^{i(k_1x_1+k_2x_2)}\sum_Q\theta(x_Q)A^Q_{a,m},$$

where $m=(m_1,m_2)$ and $a=(a_1,a_2,a_0)$ and $\mathcal{A}$ is the antisymmetrizer. The amplitudes in the various regions are connected by S matrices, e.g., $S^{01}A^{012}=A^{102}$, where S^{01}, the electron-impurity S matrix has been already determined in the one-electron problem. For this ansatz to be consistent, it must satisfy the Yang-Baxter relations

$$S^{ij}S^{i0}S^{j0}=S^{j0}S^{i0}S^{ij}, \quad (2.10)$$

guaranteeing that the two paths from (1,2,0) to (0,2,1) yield the same answer.

What is the electron-electron S matrix, S^{ij}? There is no direct electron-electron interaction term in the Hamiltonian (2.1), and one may be tempted to adopt the naive choice $S^{ij}=I$ for the scattering matrix of electrons i and j. Nevertheless, electron correlations are induced through the impurity. These show up immediately, since the naive choice does not satisfy the Yang-Baxter relations: S^{j0} and S^{i0} do not commute. This noncommutativity captures some important aspects of the model: after electron i crosses the impurity, the latter is left in a different state than before. Hence the state in which electron j finds the impurity depends on whether it crosses the impurity before or after electron i. Herein lies the difference between a system of electrons interacting with a fixed potential (a one-body problem, since all electrons ''see'' the same potential) and a Kondo system, where the impurity correlates the motion of all electrons.

Are we allowed to introduce a scattering matrix S^{ij} to satisfy the Yang-Baxter relations? We now proceed to show that this is indeed the case, namely, the introduction of an electron-electron scattering matrix would not modify the

original problem we set out to solve. Consider first the space of free electrons with a linearized Hamiltonian. The space is highly degenerate: for example the energy $E=k_1+k_2$ in the two-electron space corresponds to a wave function $F=\Sigma_q e^{i(k_1+q)x_1+i(k_2-q)x_2}A_q$ for any choice of coefficients A_q. Equivalently, we can pick a basis of the form $F=e^{ik_1x_1+ik_2x_2}[\theta(x_1-x_2)+S^{12}\theta(x_2-x_1)]A$. The choice of S^{12} is arbitrary in the two-electron space, but if we wish to proceed to construct three (and more) electron wave functions then the scattering matrices must satisfy the Yang-Baxter relations for electrons, $S^{ij}S^{ik}S^{jk}=S^{jk}S^{ik}S^{ij}$. When the Kondo interaction is turned on, the matrix S^{j0} is fixed by the interaction, which in turn picks the electron basis through the Yang-Baxter relations (2.10).

When the cutoff is present, part of the degeneracy is already removed at the free-electron level, but the procedure still goes through. Consider the model for two electrons away from the impurity.

$$h=-i\partial_j-i\partial_l+\frac{1}{2\Lambda}\partial_j^2+\frac{1}{2\Lambda}\partial_l^2+2\tilde{J}\delta(x_l-x_j)(P_{lj}-\mathcal{P}_{lj}). \tag{2.11}$$

This cutoff Hamiltonian is in the same universality class as the free linearized Hamiltonian, and possesses the same spectrum when the cutoff is sent to infinity; its particular form was chosen so that the S matrix it defines does indeed satisfy Eq. (2.10). Again, we divide configuration space into two regions:

$$F^{\{m_j,m_l\}}_{\{a_j,a_l\}}(x_j,x_l)=e^{i(k_jx_j+k_lx_l)}[A^{\{m_j,m_l\}}_{\{a_j,a_l\}}\theta(x_l-x_j)+B^{\{m_j,m_l\}}_{\{a_j,a_l\}}\theta(x_j-x_l)],$$

and study the eigenvalue equation $hF=EF$. We have

$$\begin{aligned}hF=&\left[\left(k_j-\frac{k_j^2}{2\Lambda}\right)+\left(k_l-\frac{k_l^2}{2\Lambda}\right)\right]F\\&+\left[-i(B-A)-i(A-B)+i\left(\frac{k_j}{\Lambda}-\frac{k_l}{\Lambda}\right)(B-A)\right]\\&\times\delta(x_j-x_l)e^{i(k_j+k_l)x_j}\\&+\tilde{J}(P_{jl}-\mathcal{P}_{jl})(A+B)\,\delta(x_j-x_l)e^{i(k_j+k_l)x_j}\\&+\frac{1}{2\Lambda}[(B-A)+(A-B)]\delta'(x_j-x_l)e^{i(k_jx_j+k_lx_l)}.\end{aligned} \tag{2.12}$$

The last line is identically zero; counterterms of form (2.4) are only necessary when the particles involved have different velocities. The rest of the terms proportional to $\delta(x_j-x_l)$ cancel if the amplitudes in the different regions are related by the electron-electron S matrix

$$S_{jl}=\frac{i\alpha_{jl}+\tilde{J}(P_{jl}-\mathcal{P}_{jl})}{i\alpha_{jl}-\tilde{J}(P_{jl}-\mathcal{P}_{jl})},$$

where $\alpha_{jl}\equiv(k_l-k_j)/\Lambda$. Such an S matrix can be written as

$$S_{jl}=\frac{\alpha_{jl}-2i\tilde{J}P_{jl}}{\alpha_{jl}-2i\tilde{J}}\,\frac{\alpha_{jl}+2i\tilde{J}\mathcal{P}_{jl}}{\alpha_{jl}+2i\tilde{J}}.$$

Choosing

$$\tilde{J}=\frac{J}{1+J^2}, \tag{2.13}$$

allows us to express the S matrix as

$$S_{jl}=\frac{\lambda_j-\lambda_l+icP_{jl}}{\lambda_j-\lambda_l+ic}\,\frac{\lambda_j-\lambda_l-ic\mathcal{P}_{jl}}{\lambda_j-\lambda_l-ic}. \tag{2.14}$$

The S matrices (2.9) and (2.14) satisfy the Yang-Baxter conditions (2.10), and also

$$S^{ij}S^{ik}S^{jk}=S^{jk}S^{ik}S^{ij},$$

assuring that we were able to generate a cutoff version of the Hamiltonian while maintaining integrability.

The cutoff scheme we introduced generates a flavor component in the electron-electron S matrix. Clearly it captures the interaction among electrons induced by the impurity. Already for the free Hamiltonian $\mathcal{H}_0=-i\Sigma_a^N\Sigma_m^f\int_{-\infty}^{\infty}dx\,\psi^\dagger_{a,m}(x)\partial_x\psi_{a,m}(x)$ a nontrivial S matrix *must* be introduced if we choose an SU(N)×SU(f) invariant basis (which is appropriate for a subsequent inclusion of an impurity interaction) rather than the simpler SU(fN). A careful counting of states can be carried out[7] to show that all expected states then appear with the correct degeneracies. It is instructive that this would not be the case for the naive choice $S^{ij}_{(flavor)}=I$.

The energy eigenvalues of an N^e-electron state are a generalization of the first line of Eq. (2.12). They are of the form

$$E=\sum_{j=1}^{N^e}k_j\left(1-\frac{k_j}{2\Lambda}\right). \tag{2.15}$$

C. Eigenvalue equations

In order to determine the spectrum, we impose periodic boundary conditions, and solve the corresponding eigenvalue problem. The procedure is standard,[8] and here we skip the details. The result is contained in the Bethe ansatz equations (BAE's) which we proceed to write down. Each of the degrees of freedom—charge, spin, and flavor—is described by a set of variables whose number depends on the symmetry of the particular state. The charge degrees of freedom are given by the set $\{k_j,\ j=1,\ldots,N^e\}$. The spin degrees of freedom are parameterized by the sets $\{\chi^r_\gamma,\ \gamma=1,\ldots,M^r;\ r=1,\ldots,N;\ M^N=0\}$. Finally, the flavor degrees of freedom are represented by the sets $\{\omega^r_\gamma,\ \gamma=1,\ldots,\bar{M}^r;\ r=1,\ldots,f;\ \bar{M}^f=0\}$. The set of integers $M^r;\ r=1,\ldots,N-1$ specify the symmetry of the spin component of the wave function given by an SU(N) Young tableau with the length l^r of the rth row given by $l^r=M^r-M^{r+1}$, $M^N=0$, and $M^0=N^e+1$. Similarly, the quantum numbers $\{\bar{M}^r\}$ specify the symmetry of the flavor component.

The equations are

$$e^{ik_jL}=\prod_{\gamma=1}^{M^1}\frac{\chi_\gamma^1-(1-\lambda_j)+i\frac{c}{2}}{\chi_\gamma^1-(1-\lambda_j)-i\frac{c}{2}}\prod_{\gamma=1}^{\bar{M}^1}\frac{\omega_\gamma^1-\lambda_j+i\frac{c}{2}}{\omega_\gamma^1-\lambda_j-i\frac{c}{2}}$$

$$-\prod_{\beta=1}^{\bar{M}^r}\frac{\omega_\gamma^r-\omega_\beta^r+ic}{\omega_\gamma^r-\omega_\beta^r-ic}=\prod_{t=r\pm1}\prod_{\beta=1}^{\bar{M}^t}\frac{\omega_\gamma^r-\omega_\beta^t+i\frac{c}{2}}{\omega_\gamma^r-\omega_\beta^t-i\frac{c}{2}};$$

$$r=2,\ldots,f-1,$$

$$-\prod_{\beta=1}^{\bar{M}^1}\frac{\omega_\gamma^1-\omega_\beta^1+ic}{\omega_\gamma^1-\omega_\beta^1-ic}$$

$$=\prod_{j=1}^{N^e}\frac{\omega_\gamma^1-\lambda_j+i\frac{c}{2}}{\omega_\gamma^1-\lambda_j-i\frac{c}{2}}\prod_{\beta=1}^{\bar{M}^2}\frac{\omega_\gamma^1-\omega_\beta^2+i\frac{c}{2}}{\omega_\gamma^1-\omega_\beta^2-i\frac{c}{2}},$$

$$-\prod_{\beta=1}^{M^r}\frac{\chi_\gamma^r-\chi_\beta^r+ic}{\chi_\gamma^r-\chi_\beta^r-ic}=\prod_{t=r\pm1}\prod_{\beta=1}^{M^t}\frac{\chi_\gamma^r-\chi_\beta^t+i\frac{c}{2}}{\chi_\gamma^r-\chi_\beta^t-i\frac{c}{2}};$$

$$r=2,\ldots,N-1,$$

$$-\prod_{\beta=1}^{M^1}\frac{\chi_\gamma^1-\chi_\beta^1+ic}{\chi_\gamma^1-\chi_\beta^1-ic}=\frac{\chi_\gamma^1+i\frac{c}{2}}{\chi_\gamma^1-i\frac{c}{2}}\prod_{j=1}^{N^e}\frac{\chi_\gamma^1-(1-\lambda_j)+i\frac{c}{2}}{\chi_\gamma^1-(1-\lambda_j)-i\frac{c}{2}}$$

$$\times\prod_{\beta=1}^{M^2}\frac{\chi_\gamma^1-\chi_\beta^2+i\frac{c}{2}}{\chi_\gamma^1-\chi_\beta^2-i\frac{c}{2}}.$$

The next step is to solve the equations for all possible states, and identify the ground state and the low-energy excitations. Subsequently, by summing over all excitation energies, we obtain the partition function.

The BAE's contain the cutoff Λ which eventually is sent to infinity. We shall find that in this limit the equations reduce to a smaller set once the correct ground state has been identified. It is composed of *string* solutions (see below) corresponding to electron composites which interact most efficiently with the impurity. To sharpen our intuition, we begin by some strong-coupling considerations.

1. Casimirology

As mentioned, the mechanism underlying the physics of the multichannel Kondo model is the dynamic formation of electron composites. We expect that configurations are favored which allow minimization of the local interaction at the impurity site. Consider, then, the general problem of finding the ground state of the Hamiltonian

$$J\sum_a^{N^2-1}T_a^{(e)}T_a^{(i)}, \tag{2.16}$$

where the set $\{T_a^e,\ a=1,\ldots,N^2-1\}$ is an arbitrary representation of SU(N), and $\{T_a^i,\ a=1,\ldots,N^2-1\}$ is the particular representation of the impurity, in our case it will typically be (μ). In this paper we will consider impurities with spin in a totally symmetric representation (for more general representations, see Ref. 9). Each set is normalized: $\mathrm{Tr}(T_aT_b)=\frac{1}{2}\delta_{a,b}$.

The largest number of electrons allowed at the origin by the exclusion principle is $N\times f$. This is obtained by placing N electrons in each of the channels. However, such a state is a singlet, both in spin and in flavor, and gives a zero contribution to Eq. (2.16). Therefore, the number of electrons that form the composite, M, is such that $M\leqslant(N-1)\times f$. We will show here that if the impurity is in a totally symmetric representation, the electron composite that minimizes Eq. (2.16) is made out of $M=(N-1)\times f$ electrons.

We will characterize the different representations of SU(N) by their Young tableaux. The fundamental representation is denoted by a box $\square$, and the singlet by a point $\bullet$. The totally (anti)symmetric representation resulting from the direct product of μ representations is denoted by a single (column)row made out of μ boxes, where in the antisymmetric case we assume $\mu\leqslant N$.

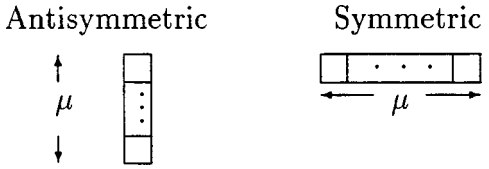

An arbitrary representation resulting from a product of M fundamentals is associated with a Young tableau made up of M boxes, distributed in $k\leqslant N$ rows. Let m_j be the number of boxes in the jth row. Then, $m_j\geqslant m_{j+1}$, $\Sigma_{j=1}^k m_j=M$. The corresponding Young tableau will be of the form

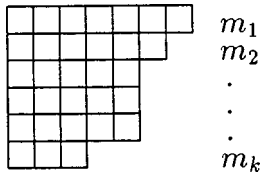

When $N=2$, the interaction (2.16) can be written in terms of conserved quantities

$$J\vec{S}^{Me}\cdot\vec{S}^i=\frac{J}{2}[S^{tot}(S^{tot}+1)-S^{Me}(S^{Me}+1)-S^i(S^i+1)]. \tag{2.17}$$

The operator $S(S+1)$ is a particular case of the Casimir operator, $C(\Gamma)$, of SU(N), which commutes with all the generators of the group. For arbitrary N,

$$J\sum_a T_a^MT_a^i=\frac{J}{2}[C(\Gamma^T)-C(\Gamma^M)-C(\Gamma^i)]. \tag{2.18}$$

Given a representation Γ of SU(N) with M boxes distributed according to the set $\{m_j\}$, we have[10]

$$C(\Gamma)=\frac{M(N^2-M)}{2N}+\frac{1}{2}\sum_{j=1}^{k} m_j(m_j+1-2j). \quad (2.19)$$

We can use Young tableaux as an easy way of decomposing the direct product of representations into a direct sum. The procedure is standard (see, for instance, Ref. 11).

The electrons will be evenly distributed among the channels, forming a flavor singlet. Hence the spin of the electron composites is described by a rectangular tableau with f columns and $k \leq N-1$ rows. Multiplying the electron tableau by the impurity tableau, we have (in the graphic representation we drop from the tableaux the singlet part consisting of columns of length N),

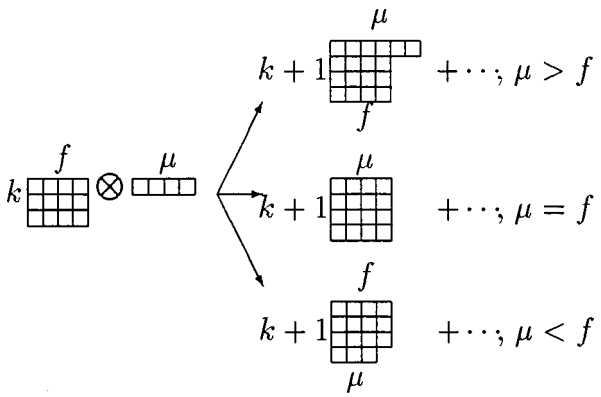

for $k<N-1$. If $k=N-1$, we have

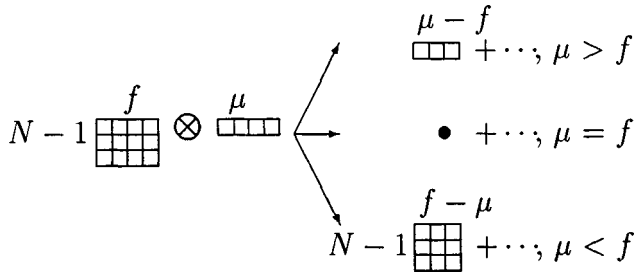

Notice that we have drawn only the terms in the decompositions that give the lowest energy. The energy for all such configurations is given by

$$J\sum_a T_a^M T_a^i=-k\frac{\min(\mu,f)}{2N}[N+\max(\mu,f)]. \quad (2.20)$$

Therefore, the energy is minimized when composites of $(N-1)\times f$ electrons are formed.

There are three different situations depending on the value of μ/f, as in the multichannel Kondo problem.[1] When $\mu>f$, there is underscreening: the electrons cannot screen the impurity completely, and the spin configuration is characterized by a Young tableau with one row and $\mu-f$ columns. As in the $N=2$ case, we will see later that such object behaves as a free spin in the Kondo problem. The second case $\mu=f$ corresponds to complete screening: the electrons and the impurity form a singlet. This is a stable fixed point of the full Hamiltonian with Fermi-liquid behavior. Finally, $\mu>f$ corresponds to overscreening: there are more electrons than necessary to screen the impurity. The resulting object corresponds to a tableau with $N-1$ columns and $f-\mu$ rows. This configuration is unstable to the kinetic term, and the fixed point in this case is characterized by non-Fermi-liquid behavior, as we will see later.

2. Fusion

We turn now to the dynamics of the full model captured by the BAE. We shall argue that the ground state and low-lying excitations lie in a sector of the theory given by solutions of a particular form—*f strings*. Solutions of this type are SU(f) flavor singlets—allowing them to have maximally large SU(N) spin. We shall find that this class of excitations is characterized by a scale $T_0=De^{-2\pi/Nc}$. When strings are broken to form flavored excitations, we expect them to be characterized by other scales which will tend to infinity as the cutoff is removed, and thus not contribute to the impurity dynamics.[7]

The formation of composites in flavor corresponds to solutions of the BAE where the charge parameters, $\{\lambda_j\}$, are complex numbers centered around $\{\omega_\gamma^1\}$, according to the string hypothesis.[12,13] Likewise, rank r flavor parameters are themselves centered around rank $r+1$ solutions.[6] The form of the charge parameters is

$$\lambda_\delta^q=\frac{p_\delta}{\Lambda}+ic\left(\frac{f+1}{2}-q\right), \quad q=1,2,\ldots,f, \quad p_\delta \ real.$$

while the flavor parameters,

$$\{\omega_\gamma^r,\gamma=1,2,\ldots,M^r\}=\{p_A/\Lambda+iJ[(f-r+1)/2-q],$$

$$q=1,2,\ldots,f-r,A=1,\ldots,N\},$$

where $r=0,1,\ldots,f-1$. These configurations satisfy the BAE in a trivial manner, and induce *fusion* in the BAE equations as well as in the form of the wave functions. A string built on momentum p as its real part induces in the wave function a composite of the form $\exp\{-\frac{1}{2}\Lambda J\Sigma_{j,l}|x_j-x_l|+ip(x_1+\cdots x_f)\}\times[\cdots]$, which becomes local as $\Lambda\to\infty$.

Inserting the string configurations into the full BAE, we obtain the effective equations governing the impurity spin dynamics. After removing the cutoff, they become

$$e^{ifp_\delta L}=\prod_{\gamma=1}^{M^1}\frac{\chi_\gamma^1-1+if\frac{c}{2}}{\chi_\gamma^1-1-if\frac{c}{2}},$$

$$-\prod_{\beta=1}^{M^r}\frac{\chi_\gamma^r-\chi_\beta^r+ic}{\chi_\gamma^r-\chi_\beta^r-ic}=\prod_{t=r\pm1}\prod_{\beta=1}^{M^t}\frac{\chi_\gamma^r-\chi_\beta^t+i\frac{c}{2}}{\chi_\gamma^r-\chi_\beta^t-i\frac{c}{2}},$$

$$r=2,\ldots,N-1,$$

$$-\prod_{\beta=1}^{M^1}\frac{\chi_\gamma^1-\chi_\beta^1+ic}{\chi_\gamma^1-\chi_\beta^1-ic}=\frac{\chi_\gamma^1+i\frac{c}{2}}{\chi_\gamma^1-i\frac{c}{2}}\prod_{\delta=1}^{N^e/f}\frac{\chi_\gamma^1-1+if\frac{c}{2}}{\chi_\gamma^1-1-if\frac{c}{2}}\times\prod_{\beta=1}^{M^2}\frac{\chi_\gamma^1-\chi_\beta^2+i\frac{c}{2}}{\chi_\gamma^1-\chi_\beta^2-i\frac{c}{2}},$$

and the energy is given by

$$E=\sum_{\delta=1}^{N^e/f} fp_\delta.$$

We now proceed to discuss the solutions of the fused equations. The solutions for the rank r spin variables $\{\chi^r\}$ again fall into strings of arbitrary length n,

$$\chi_{\gamma,j}^{r,n}=\chi_\gamma^{r,n}+i\frac{c}{2}(n+1-2j),\quad j=1,\ldots,n,\quad n=1,\ldots,\infty.$$

and a state is characterized by the quantum numbers $M^{r,m}$ specifying the number of length-m strings of rank r ($\Sigma_{m=1}^{\infty}mM^{r,m}=M^r$).

The equations coupling the real part of the strings, after summing over the complex variables, can be conveniently written down in a logarithmic form. Let us first introduce the following definitions:

$$\theta_n(x)\equiv-2\arctan\left(\frac{2}{nc}x\right),$$

$$\phi_{n,m}^k(x)\equiv\sum_{j=1}^{\min(n,m)}\theta_{m+n+k-2j}(x),$$

$$\phi_{n,m}^0(x)\equiv\sum_{j=1}^{\min(n-1,m-1)}\theta_{m+n-2j}(x).$$

Then, after some manipulations the Bethe ansatz equations take the form

$$\sum_{m=1}^{\infty}\sum_{\beta=1}^{M^{r,m}}[\phi_{n,m}^2(\chi_\gamma^{r,n}-\chi_\beta^{r,m})+\phi_{n,m}^0(\chi_\gamma^{r,n}-\chi_\beta^{r,m})]$$

$$=2\pi I_\gamma^{r,n}+\sum_{l=1}^{\infty}\sum_{\beta=1}^{M^{r-1,l}}\phi_{n,l}^1(\chi_\gamma^{r,n}-\chi_\beta^{r-1,l})+\sum_{l=1}^{\infty}\sum_{\beta=1}^{M^{r+1,l}}\phi_{n,l}^1(\chi_\gamma^{r,n}-\chi_\beta^{r+1,l}),$$

$$\sum_{m=1}^{\infty}\sum_{\beta=1}^{M^{1,m}}[\phi_{n,m}^2(\chi_\gamma^{1,n}-\chi_\beta^{1,m})+\phi_{n,m}^0(\chi_\gamma^{1,n}-\chi_\beta^{1,m})]$$

$$=2\pi I_\gamma^{1,n}+\phi_{n,1}^1(\chi_\gamma^{1,n})+\frac{N^e}{f}\phi_{n,f}^1(\chi_\gamma^{1,n}-1)+\sum_{l=1}^{\infty}\sum_{\beta=1}^{M^{2,l}}\phi_{n,l}^1(\chi_\gamma^{1,n}-\chi_\beta^{2,l}).$$

The expression for the energy of the spin and charge sector is given by

$$E=\sum_{\delta=1}^{N^e/f}\frac{2\pi}{L}m_\delta+\frac{D}{f}\sum_{n=1}^{\infty}\sum_{\beta=1}^{M^{1,n}}[\phi_{n,f}^1(\chi_\gamma^{1,n}-1)-\pi\min(n,f)],$$

where $D=N^e/L$ is the electron density. It will turn out also to play the role of the cutoff. In the presence of a magnetic field H, there is a contribution to the energy of the form

$$-2H\sum_{k=0}^{N-1}(M^k-M^{k+1})\left(\frac{N-1}{2}-k\right)=-2H\left(\frac{N-1}{2}(N^e+1)-\sum_{r=1}^{N}M^r\right).$$

We now take the thermodynamic limit $N^e\to\infty$ and $L\to\infty$, holding D finite. In the limits we may replace sums with integrals after introducing densities of solutions, $\sigma_n^r(\chi)$, and densities of holes in the distribution of solutions, $\sigma_n^{r,h}(\chi)$. The energy is now written as

$$E=E_c-H(N-1)(N^e+1)+\sum_{n=1}^{\infty}\sum_{r=1}^{N-1}\int_{-\infty}^{\infty}d\chi\ \sigma_n^r(\chi)g_{r,n}(\chi),$$

where we introduced the energy function,

$$g_{r,n}(\chi)=\frac{D}{f}[\phi_{n,f}^1(\chi-1)-\pi\min(n,f)]\delta_{r,1}+2Hn,$$

and E_c denotes the contribution of the charge sector to the energy,

$$E_c=\sum_{\delta=1}^{N^e/f}\frac{2\pi}{L}m_\delta.$$

In the thermodynamic limit the BAE's are replaced by integral equations for the densities, $\{\sigma_n^r,\sigma_n^{r,h}\}$. Standard manipulations[8] lead to

$$\sigma_n^{r,h}(\chi)=-\sum_{m=1}^{\infty}\sum_{s=0}^{N}\int_{-\infty}^{\infty}d\chi' A_{n,m}^{r,s}(\chi-\chi')\sigma_m^s(\chi'),$$

where we introduced the following operators:

$$K^{\alpha}_{n,m}(\chi)\equiv \sum_{j=1}^{\min(n,m)} k_{m+n+\alpha-2j}(\chi),$$

$$\tilde{K}^{0}_{n,m}(\chi)\equiv \sum_{j=1}^{\min(n-1,m-1)} k_{m+n-2j}(\chi),$$

$$k_{\alpha}(\chi)\equiv -\frac{1}{2\pi}\theta_{\alpha}(\chi), \quad k_0(\chi)\equiv\delta(\chi);$$

and

$$A_{n,m}(\chi)\equiv K^{2}_{n,m}(\chi)+K^{0}_{n,m}(\chi),$$

$$B_{n,m}(\chi)\equiv K^{1}_{n,m}(\chi),$$

$$A^{r,s}_{n,m}\equiv A_{n,m}\delta^{r,s}-B_{n,m}(\delta^{r,s+1}+\delta^{r,s-1}), \quad r\geqslant 1;$$

and, by convention,

$$\sigma^{0}_{l}(\chi)\equiv\delta(\chi)\delta_{l,1}+\frac{N^{e}}{f}\delta(\chi+1)\delta_{l,f}, \tag{2.21}$$

$$\sigma^{N}_{n}(\chi)\equiv 0. \tag{2.22}$$

We shall not analyze the ground state and individual excitations here. Instead, we shall proceed to derive the thermodynamic properties of the model.

III. THERMODYNAMICS

A. Thermodynamic Bethe ansatz equations

We now calculate the impurity contribution to the free energy, using the well-known formalism of Refs. 12 and 13. We seek to find the configuration $\{\sigma^{r}_{n}(\chi)+\sigma^{r,h}_{n}(\chi)\}$, which would extremize the free energy. The entropy of such a configuration is

$$\mathcal{S}=\sum_{n,r}\int d\chi\{[\sigma^{r}_{n}(\chi)+\sigma^{r,h}_{n}(\chi)]\ln[\sigma^{r}_{n}(\chi)+\sigma^{r,h}_{n}(\chi)] - \sigma^{r}_{n}(\chi)\ln\sigma^{r}_{n}(\chi)-\sigma^{r,h}_{n}(\chi)\ln\sigma^{r,h}_{n}(\chi)\},$$

and its contribution to the spin free energy

$$F=E-T\mathcal{S}=-H(N-1)(N^{e}+1)+\sum_{n,r}\int d\chi\{\sigma^{r}_{n}(\chi)g_{r,n}(\chi) - T[(\sigma^{r}_{n}(\chi)+\sigma^{r,h}_{n}(\chi))\ln[\sigma^{r}_{n}(\chi)+\sigma^{r,h}_{n}(\chi)] - \sigma^{r}_{n}(\chi)\ln\sigma^{r}_{n}(\chi)-\sigma^{r,h}_{n}(\chi)\ln\sigma^{r,h}_{n}(\chi)]\}.$$

The free energy is varied with respect to the densities, subject to constraints imposed by the Bethe ansatz equations

$$\delta\sigma^{r,h}_{n}(\chi)=-\sum_{m,s}\int_{-\infty}^{\infty}d\chi' A^{r,s}_{n,m}(\chi-\chi')\delta\sigma^{s}_{m}(\chi'),$$

$$\delta\sigma^{0}_{n}(\chi)=\delta\sigma^{N}_{n}(\chi)=0.$$

We obtain the following infinite set of integral equations for the equilibrium densities:

$$\ln[1+\eta^{r}_{n}(\chi)]=\frac{g_{r,n}(\chi)}{T}+\sum_{m,s}\int_{-\infty}^{\infty}d\chi' A^{r,s}_{n,m}(\chi-\chi') \times\ln[1+(\eta^{s}_{m}(\chi'))^{-1}], \tag{3.1}$$

where

$$\eta^{r}_{n}(\chi)\equiv\frac{\sigma^{r,h}_{n}(\chi)}{\sigma^{r}_{n}(\chi)}, \quad (\eta^{N}_{n})^{-1}\equiv(\eta^{0}_{n})^{-1}\equiv 0.$$

We transform this set of equations with the help of the identities (we will now drop the functional dependence)

$$A^{r,s}_{n,m}-G(A^{r,s}_{n-1,m}+A^{r,s}_{n+1,m}) =\delta_{n,m}\delta^{r,s}-G\delta_{n,m}(\delta^{r,s+1}+\delta^{r,s-1})$$

$$A^{r,s}_{1,m}-GA^{r,s}_{2,m}=\delta_{1,m}\delta^{r,s}-G\delta_{1,m}(\delta^{r,s+1}+\delta^{r,s-1}),$$

with the integral operator G defined as

$$Gf(\chi)\equiv\frac{[1]}{[0]+[2]}f(\chi)\equiv\frac{1}{2c}\int_{-\infty}^{\infty}d\chi'\frac{f(\chi')}{\cosh\left(\frac{\pi}{c}(\chi-\chi')\right)},$$

and $[n]f(\chi)\equiv\int_{-\infty}^{\infty}d\chi' k_n(\chi-\chi')f(\chi')$. We find

$$\ln\eta^{r}_{1}=-\frac{2}{f}\frac{D}{T}\arctan e^{\pi/c(\chi-1)}\delta^{r,1}\delta_{n,f}+G\ln(1+\eta^{r}_{1}) - G[\ln(1+(\eta^{r-1}_{1})^{-1})+\ln(1+(\eta^{r+1}_{1})^{-1})], \tag{3.2}$$

$$\ln\eta^{r}_{n}=-2\frac{D}{Tf}\arctan e^{(\pi/c)(\chi-1)}\delta^{r,1}\delta_{n,f}+G[\ln(1+\eta^{r}_{n-1}) +\ln(1+\eta^{r}_{n+1})]-G[\ln(1+(\eta^{r-1}_{n})^{-1}) +\ln(1+(\eta^{r+1}_{n})^{-1})], \tag{3.3}$$

with boundary conditions,

$$\lim_{n\to\infty}\{[n+1]\ln(1+\eta^{r}_{n})-[n]\ln(1+\eta^{r}_{n+1})\}=-2\frac{H}{T}, \tag{3.4}$$

which follow directly from Eq. (3.1). Another form of these equation can be obtained after inverting, (see Ref. 12),

$$-\ln(1+(\eta^{r}_{n})^{-1})=-\frac{\Delta E^{fund}_{N,r}}{T}\delta_{n,f}+\sum_{q=1}^{N-1}G^{r,q}_{N}[\ln(1+\eta^{q}_{n+1}) +\ln(1+\eta^{q}_{n-1})-G^{-1}\ln(1+\eta^{q}_{n})], \tag{3.5}$$

where $\ln(1+\eta^{r}_{0})\equiv 0$, and the Fourier transform of the kernel of the integral operator $G^{r,q}_{N}$ is given by

$$\tilde{G}^{r,q}_{N}(p)\equiv\frac{\sinh\left(\min(r,q)\frac{cp}{2}\right)\sinh\left([N-\max(r,q)]\frac{cp}{2}\right)}{\sinh\left(\frac{cp}{2}\right)\sinh\left(N\frac{cp}{2}\right)}.$$

The driving term in these equations,

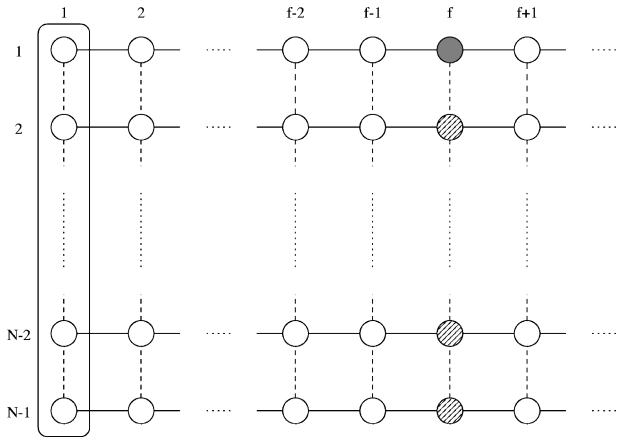

FIG. 1. Diagrammatic representation of the integral equations. The circles correspond to the functions η_n^r. The filled circle indicates that the equation for the corresponding η_n^r has a driving term. The circles with stripes indicate that the corresponding η_n^r have driving terms in the other set of TBA equations. The solid line indicates a link between two η_n^r through the convolution G ln(1 $+\eta$). The dashed line indicates a link through G ln(1+1/η). Finally, the box encircles η_1^r, which is the function used to evaluate the impurity contribution to the free energy.

$$\Delta E_{N,r}^{fund}=G_N^{r,1}G^{-1}\left(2\frac{D}{f}\arctan\, e^{(\pi/c)(\chi-1)}\right),$$

is the energy of the fundamental excitation. It can be calculated explicitly:

$$\Delta E_{N,r}^{fund}=\frac{D}{f}\left\{\pi\frac{N-r}{N}-2\arctan\left[\tan\left(\frac{\pi}{2}\frac{N-r}{N}\right)\times\tanh\left(\frac{\pi}{Nc}(\chi-1)\right)\right]\right\}.$$

A pictorial description of Eq. (3.5) is shown in Fig. 1. The circles correspond to the functions $\eta_n^r(x)$, and are arranged according to their indices. The lines join functions that appear in the same equation. The full and dotted lines indicate that the functions $\eta_n^{r\pm1}$ and $\eta_{n\pm1}^r$ appear differently in Eqs. (3.2) and (3.3). The driving terms in Eqs. (3.2) and (3.3) correspond to filled dark circles in Fig. 1. The diagonally lined circles correspond to functions associated to a driving term in Eq. (3.5). Clearly there are two regions: one, $n<f$, contains a finite number of functions η_n^r; while the other, $n>f$, is unbounded. The regions are separated by the column with the driving terms, $n=f$. When studying the low-T properties of the system, we will only need to consider one region at a time.

We will now write the free energy in terms of the set $\{\eta_n^r\}$. Using the integral equations for the densities we can write

$$F=F_0+\sum_{n,r}\int d\chi\left(g_{r,n}\sigma_n^r-T\sigma_n^r\ln(1+\eta_n^r)+T\sum_{m,s}\int d\chi' A_{n,m}^{r,s}\sigma_n^r\ln[1+(\eta_m^s)^{-1}]\right),$$

where $F_0=E_c-H(N-1)(N^e+1)$ is the ground-state energy. After a few further manipulations, the free energy can be written as

$$F=F_0-T\sum_n\int_{-\infty}^{\infty}d\chi\,\ln(1+(\eta_n^1)^{-1})\times\left\{k_n(\chi)+\frac{N^e}{f}\sum_{j=1}^{\min(n,f)}k_{f+n+1-2j}(\chi-1)\right\}.$$

We are only interested in the impurity contribution to the free energy, F^i, which contains all the effects of the interaction. It is

$$F^i=-T\sum_{n=1}^{\infty}\int_{-\infty}^{\infty}d\chi\,\delta(\chi)[n]\ln[1+(\eta_n^1)^{-1}]=\sum_{q=1}^{N-1}\int_{-\infty}^{\infty}d\chi G_N^{1,q}(\chi)g_1^q(\chi)-T\sum_{q=1}^{N-1}\int_{-\infty}^{\infty}d\chi\,G_N^{1,q}(\chi)\times\ln(1+\eta_1^q).$$

The first term corresponds to the impurity contribution to the ground state. At finite temperatures we are only interested in the second term, which after further manipulations becomes

$$F^i=-T\sum_{q=1}^{N-1}\int_{-\infty}^{\infty}d\chi\frac{1}{Nc}\frac{\sin\,\pi\dfrac{N-q}{N}}{\cosh\dfrac{2\pi\chi}{Nc}+\cos\,\pi\dfrac{N-q}{N}}\times\ln[1+\eta_1^q(\chi)].$$

When the impurity is in the fundamental representation, only the η_1^r functions contribute to F^i. In Fig. 1, this feature corresponds to a box drawn around the first column.

B. Scaling limit

We will now take the scaling limit, $D\to\infty$, $c\to0$, T_0 constant, where

$$T_0=De^{-2\pi/Nc}.$$

This is the correct limit as discussed in Ref. 12. We also introduce the variable

$$\xi=\frac{2\pi}{Nc}\chi+\ln\frac{T_0}{T},$$

so

$$F^i=-\frac{T}{2\pi}\sum_{q=1}^{N-1}\int_{-\infty}^{\infty}d\xi\frac{\left(\sin\,\pi\dfrac{N-q}{N}\right)\ln[1+\eta_1^q(\xi)]}{\cosh\left(\xi-\ln\dfrac{T_0}{T}\right)+\cos\,\pi\dfrac{N-q}{N}}.\tag{3.6}$$

The only modification in the thermodynamic equations is in $\Delta E_{N,r}^{fund}$. Thus

$$-\ln(1+(\eta_n^r)^{-1}) = -\frac{2}{f}e^{\xi}\sin\left(\frac{\pi r}{N}\right)\delta_{n,f} + \sum_{q=1}^{N-1} G_N^{r,q}[\ln(1+\eta_{n+1}^q) + \ln(1+\eta_{n-1}^q) - G^{-1}\ln(1+\eta_n^q)], \tag{3.7}$$

$$\eta_0^r \equiv 0, \quad \ln[1+(\eta_n^0)^{-1}] \equiv 0, \quad \ln[1+(\eta_n^f)^{-1}] \equiv 0, \tag{3.8}$$

with boundary conditions

$$\lim_{n\to\infty}\{[n+1]\ln(1+\eta_n^r) - [n]\ln(1+\eta_{n+1}^r)\} = -2\frac{H}{T}. \tag{3.9}$$

C. Asymptotic solutions—low-temperature properties

Here we will study several asymptotic limits of the thermodynamic integral equations. Some technical points will be considered in detail. It is not easy to study analytically the integral equations (3.7)–(3.9) due to the complexity of the operator $G_N^{r,q}$. Instead, we will study the equivalent set equations (3.2)–(3.4). We will discuss the appropriate procedure to obtain the asymptotic solutions of the equations order by order. The zeroth-order approximation yields a description of the fixed point itself, and the corrections (first order) describe its neighborhood.

1. Zeroth order—the fixed point

The functions η_n^r tend either to 0 or to constant values as the magnitudes of their arguments tend to infinity. The only information needed about the driving term is that it tends to 0 as $\xi\to-\infty$, and to $-\infty$ as $\xi\to\infty$. Therefore, the parameter χ does not appear explicitly in Eqs. (3.2)–(3.4), and the kernel of G can be replaced by $\frac{1}{2}\delta(\xi-\xi')$.

Thus the zeroth-order problem consists in evaluating the set of constants

$$\eta_n^{r,\pm} \equiv \eta_n^r(\xi\to\pm\infty).$$

When $\xi\to-\infty$, all the driving terms vanish, and the algebraic equations for the set $\{\eta_n^{r,-}\}$ are

$$2\ln\eta_n^{r,-} = \ln(1+\eta_{n+1}^{r,-}) + \ln(1+\eta_{n-1}^{r,-}) + \ln[1+(\eta_n^{r+1,-})^{-1}] + \ln[1+(\eta_n^{r-1,-})^{-1}],$$

$$\eta_0^{r,-} = 0,$$

$$\ln[1+(\eta_n^{0,-})^{-1}] = \ln[1+(\eta_n^{N,-})^{-1}] = 0,$$

$$-2\frac{H}{T} = \lim_{n\to\infty}\{[n+1]\ln(1+\eta_n^{r,-}) - [n]\ln(1+\eta_{n+1}^{r,-})\},$$

Since the kernel of $G_N^{r,q}(\chi)$ satisfies

$$G_N^{r,q} = G_N^{q,r}, \quad G_N^{r,q} = G_N^{N-r,N-q},$$

we must have $\eta_n^{N-r} = \eta_n^r$. The solution is easily obtained, as it is independent of the flavor symmetry,

$$\eta_n^{r,-} = \frac{\sinh[(n+r)x_0]\sinh[(n+N-r)x_0]}{\sinh(rx_0)\sinh[(N-r)x_0]} - 1, \tag{3.10}$$

$$n=1,2,\ldots, \quad r=1,\ldots,N-1, \quad x_0=\frac{H}{T}.s$$

As for $\eta_n^{n,+}$, we should consider separately the cases $n>f$ and $n<f$ ($\eta_f^{r,+}=0$). In the first case, we have equations similar to those for $\{\eta_n^{r,-}\}$, except that all the indices n are *shifted* by f, in analogy with the multichannel Kondo model. Hence

$$\eta_n^{r,+} = \frac{\sinh[(n-f+r)x_0]\sinh[(n-f+N-r)x_0]}{\sinh(rx_0)\sinh[(N-r)x_0]} - 1,$$

$$n=f,f+1,\ldots, \quad r=1,\ldots,N-1. \tag{3.11}$$

Finally, for $n<f$ there are a finite number of $\eta_n^{r,+}$ involved, since $\eta_f^{r,+}=0$, and $G\ln(1+\eta_f^r)=0$. As in the multichannel Kondo model,[6] the *sinh* functions are replaced by *sin* functions, and the coefficients are independent of the magnetic field. Thus

$$\eta_n^{r,+} = \frac{\sin\left(\frac{\pi}{(f+N)}(n+r)\right)\sin\left(\frac{\pi}{(f+N)}(n+N-r)\right)}{\sin\left(\frac{\pi}{(f+N)}r\right)\sin\left(\frac{\pi}{(f+N)}(N-r)\right)} - 1,$$

$$n=1,\ldots,f-1, \quad r=1,\ldots,N-1. \tag{3.12}$$

These results coincide with those obtained in Ref. 14 for a model of interacting fermions with the same symmetry. This is not surprising, since these results depend only on the symmetry of the problem. Notice that the multichannel Kondo results correspond to Eqs. (3.10)–(3.12) with $N=2$. Some features of Eqs. (3.10)–(3.12) can be appreciated in Fig. 1. When $\xi\to-\infty$, the driving term does not contribute to the equations, and the situation is the same as in the Coqblin-Schrieffer model. For $\xi\to\infty$, and $n\geqslant f$, we can disregard the $n<f$ sector, and the leftover diagram is effectively the same as for the Coqblin-Schrieffer model with the substitution $n\to n-f$. Finally, for $n<f$, we have a finite number of $\eta_n^{r,+}$ involved. Hence the replacement of the sinh by sin.

2. Residual entropy—the fixed point

Here we will calculate the residual entropy in the overscreened case, $f>1$. As $T\to0$, the dominant term in the free energy will be linear, and it will depend only on the values of $\eta_1^{r,+}$.

$$F^i \sim -\frac{T}{2\pi}\sum_{q=1}^{N-1}\sin\left(\pi\frac{N-q}{N}\right) \tag{3.13}$$

$$\times\int_0^\infty d\xi\frac{\ln(1+\eta_1^{q,+})}{\cosh\left(\xi-\ln\frac{T_0}{T}\right)+\cos\left(\pi\frac{N-q}{N}\right)} \tag{3.14}$$

$$\sim -T\sum_{q=1}^{N-1}\left(\frac{N-q}{N}\right)\ln(1+\eta_1^{q,+}). \tag{3.15}$$

Substituting the values of $\eta_1^{q,+}$, and taking advantage of the symmetry that $\eta_1^{N-q,+}=\eta_1^{q,+}$, we find

$$F^i=-T\,\ln\frac{\sin\dfrac{\pi N}{f+N}}{\sin\dfrac{\pi}{f+N}}.$$

Hence the residual entropy is

$$S^i_{T=0}=-\left.\frac{\partial F^i}{\partial T}\right|_{T=0}=\ln\frac{\sin\dfrac{\pi N}{f+N}}{\sin\dfrac{\pi}{f+N}}=\ln\frac{\sin\dfrac{\pi f}{f+N}}{\sin\dfrac{\pi}{f+N}}. \tag{3.16}$$

Once again, we recover the multichannel results if we set $N=2$. It is quite clear that it is not the logarithm of an integer number.

The expression for the entropy can be written as the sum of two terms: one that depends only on $N+f$ and a second one that depends only on $|\ln\,\gamma|$, ($\gamma=f/N$)

$$S^i=\ln\sin\frac{\pi}{1+e^{|\log\,\gamma|}}-\ln\sin\frac{\pi}{N+f}. \tag{3.17}$$

In the limits $f\gg N$ and $f\ll N$, we have

$$S^i=\begin{cases}\ln N-\dfrac{\pi^2}{6}\dfrac{N^2-1}{f^2}, & f\gg N,\\[2ex] \ln f-\dfrac{\pi^2}{6}\dfrac{f^2-1}{N^2}, & f\ll N.\end{cases} \tag{3.18}$$

Furthermore, it is clear from Eq. (3.17) that two systems characterized by γ_1 and γ_2, such that $\gamma_1=1/\gamma_2$, have the same residual entropy. When $\gamma=1$, the first term is zero.

Figure 2 corresponds to (3.16) for different values of N and f. It is quite apparent that the value of S^i increases with $N+f$. It is also clear that the figure is symmetric with respect to the $N=f$ axis, which means that S^i is the same for γ and for $1/\gamma$. Finally, if we fix $N+f$, the largest value of the residual entropy corresponds to $N=f$.

In terms of the diagrammatic construction, Fig. 1, S^i measures the size of the overscreened region and how asymmetric the region is. For fixed $N+f$, the largest residual entropy corresponds to $\gamma=1$, in the same way as the square is the rectangle with the largest area for a fixed perimeter. This can be seen in the following diagrams, were we have omitted the lines and drawn only the circles corresponding to $n<f$.

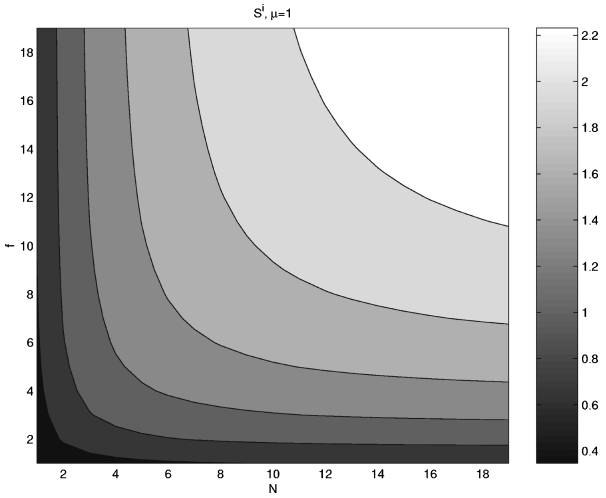

FIG. 2. Overscreening residual entropy S^i for an impurity in the fundamental representation of SU(N), and for different values of N and f.

$N=7, f=3$

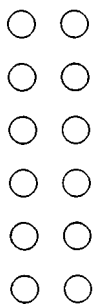

(3.19)

$N=f=5$

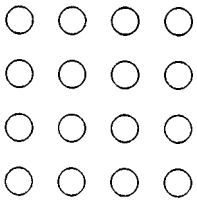

(3.20)

$N=3, f=7$

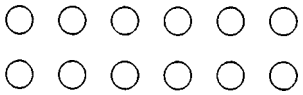

(3.21)

The largest entropy corresponds to the configuration with the largest number of circles, for a fixed value of $N+f$. That is, $N=f$. Notice that the first and the third cases have the same number of circles and, indeed, the same value of of the impurity entropy S^i.

3. First order–the neighborhood of the fixed point

Now we turn to the calculation of the thermodynamic properties of the SU(N)×SU(f) model well below the Kondo scale T_0. As is obvious from Eq. (3.14) for $T\ll T_0$, the nontrivial temperature dependence of the impurity free

energy is determined by the asymptotic behavior of the functions $\eta_1^q(\xi)$ in the region $\xi \gg 1$. Therefore, we want to find the dominant dependence of η_n^r on ξ for $n<f$ and ξ large and positive. To this purpose we will only need the equations with $n<f$, which do not have a driving term, and the asymptotic value of η_f^r.

Consider the action of the operator G

$$G_\chi f = \frac{1}{2c}\int_{-\infty}^{\infty} d\chi' \frac{f(\chi')}{\cosh\left(\frac{\pi}{c}(\chi-\chi')\right)},$$

$$= \frac{1}{2c}\int_{-\infty}^{\infty} d\chi' \frac{\tilde{f}\left(\frac{2\pi\chi'}{Nc}+\ln\frac{T_0}{T}\right)}{\cosh\left(\frac{N}{2}\frac{2\pi}{Nc}(\chi-\chi')\right)},$$

$$= \frac{N}{4\pi}\int_{-\infty}^{\infty} d\xi' \frac{\tilde{f}(\xi')}{\cosh\left(\frac{N}{2}(\xi-\xi')\right)} \equiv G_\xi f,$$

where we have dropped the tilde in the last expression. This establishes the correspondence between functions and variables of the two systems of equations.

From the set of equations (3.2)–(3.4), and the asymptotic values (3.7)–(3.9) we learn that for large and positive values of ξ we have (if $x_0 = H/T$ is very small)

$$\eta_f^r(\xi) \propto (\alpha^r + \beta^r x_0^2)\exp\left\{-\frac{2}{f}\sin\left(\frac{\pi r}{N}\right)e^{\xi}\right\}. \quad (3.22)$$

We now evaluate the dominant contribution to $G_\xi \ln(1+\eta_f^r)$,

$$G_\xi \ln(1+\eta_f^r) = \frac{N}{4\pi}\int_{-\infty}^{\infty} d\xi' \frac{\ln(1+\eta_f^r)}{\cosh\frac{N}{2}(\xi-\xi')},$$

$$\overset{\xi\gg 1}{\sim} \frac{N}{4\pi}(\alpha^r+\beta^r x_0^2)\int_{\omega}^{\infty} d\xi' \frac{e^{-\Delta e^{\xi'}}}{\cosh\frac{N}{2}\xi'},$$

where ω is some lower cutoff of the integral of the order of unity, and

$$\Delta \equiv \frac{2}{f}\sin\left(\frac{\pi r}{N}\right)e^{\xi}.$$

For large ξ, the only relevant contribution to the integral occurs around $e^{\xi'} \sim 1/\Delta$. Therefore, we approximate the previous integral by

$$(\alpha^r+\beta^r x_0^2)\frac{\Delta^{N/2}}{1+\Delta^N} \sim (\alpha^r+\beta^r x_0^2)e^{-(N/2)\xi}.$$

Notice that this is correct up to terms of the form $\xi^\mu e^{-(N/2)\xi}$ which cannot be accounted for using this crude approximation.

The previous calculation indicates that $\eta_{n<f}^r$ will have a contribution of order $e^{-(N/2)\xi}$, since $G_\xi e^{-\alpha\xi} \propto e^{-\alpha\xi}$, as we will see below. Therefore, we have to determine whether there are contributions more singular still. In other words, we have to find out if there are solutions of the integral equations for large ξ of the form

$$\eta_{n<f}^r(\xi) \sim \eta_{n<f}^{r,+} + c_n^r(\alpha^r+\beta^r x_0^2)e^{-\tau\xi} \quad \text{with} \quad \tau < \frac{N}{2}.$$

Introducing the eigenvalue $\lambda \equiv 2\cos\pi\tau/N$, so that

$$Ge^{-\tau\xi} = \frac{e^{-\tau\xi}}{\lambda}$$

we proceed to convert the thermodynamic Bethe ansatz (TBA) equations into algebraic recursion relations. Noting that

$$\ln(1+\eta_n^r) \sim \ln(1+\eta_n^{r,+}) + (b_n^r + a_n^r x_0^2)e^{-\tau\xi},$$

$$\ln\ \eta_n^r \sim \ln_n^{r,+} + \frac{(b_n^r + a_n^r x_0^2)}{\omega_n^r}e^{-\tau\xi}$$

where

$$(b_n^r + a_n^r x_0^2) \equiv \frac{c_n^r(\alpha^r+\beta^r x_0^2)}{1+\eta_n^{r,+}}$$

$$\omega_n^r \equiv \frac{\eta_n^{r,+}}{1+\eta_n^{r,+}}$$

then substituting in the integral equations (3.2) and (3.3) for $n<f$ and using the zeroth-order results, we obtain the following set of algebraic equations for the coefficients of $e^{-\tau\xi}$ (we only write the equations for b_n^r since they are identical to those for a_n^r):

$$\lambda b_n^r = \omega_n^r(b_{n+1}^r + b_{n-1}^r) + \frac{\omega_n^r}{\eta_n^{r+1,+}}b_n^{r+1} + \frac{\omega_n^r}{\eta_n^{r-1,+}}b_n^{r-1},$$

with

$$b_0^r = b_f^r = 0. \quad (3.23)$$

More explicitly, upon inserting zero-order values, the equations become,

$$\lambda b_n^r = \frac{\sin[(n+N)a]\sin(na)}{\sin[(n+r)a]\sin[(n+N-r)a]}(b_{n+1}^r + b_{n-1}^r) + \frac{\sin[(r+1)a]\sin[(N-r-1)a]}{\sin[(n+r)a]\sin[(n+N-r)a]}b_n^{r+1} + \frac{\sin[(r-1)a]\sin[(N-r+1)a]}{\sin[(n+r)a]\sin[(n+N-r)a]}b_n^{r-1}, \quad (3.24)$$

where

$$a \equiv \frac{\pi}{f+N}.$$

We solve Eq. (3.24) by inspection. Since b_n^r has to satisfy the *boundary conditions*, [Eq. (3.23)], we have that

$$b_n^r = \sin[(n+N)a]\sin(na)d_n^r$$

is the maximal solution when $d_n^r = d = \text{const}$, and the eigenvalue is

$$\lambda = 2\cos\frac{\pi\tau}{N} = 2\cos\frac{2\pi}{f+N}. \tag{3.25}$$

Hence, finally,

$$\tau = \frac{2N}{N+f}. \tag{3.26}$$

We shall see in Sec. III D 4 that τ is the main critical exponent in the model.

4. Specific heat and finite-temperature susceptibility

The expression for the impurity contribution to the free energy, F^i, at low temperatures always has a term which is proportional to T^2. This contribution comes from the term proportional to $e^{-(N/2)\xi}$ present in $\eta^r_{n<f}$, as we discussed in Sec. III D3.

Here, we will study contributions of the form

$$\Delta F^i \propto -\frac{T}{2\pi}\int_{-\infty}^{\infty} d\xi \sum_{q=1}^{N} \frac{\sin\left(\pi\frac{N-q}{N}\right)(\alpha^q+\beta^q x_0^2)e^{-\tau\xi}}{\cosh\left(\xi-\ln\frac{T_0}{T}\right)+\cos\pi\frac{N-q}{N}} = -\frac{T}{2\pi}\left(\frac{T}{T_0}\right)^{\tau}\int_{-\infty}^{\infty} d\xi \sum_{q=1}^{N} \frac{\sin\left(\pi\frac{N-q}{N}\right)(\alpha^q+\beta^q x_0^2)e^{-\tau\xi}}{\cosh(\xi)+\cos\pi\frac{N-q}{N}}, \tag{3.27}$$

which might become dominant depending on the value of τ. We will consider the three cases $f>N$, $f=N$, and $f<N$ separately.

Case $f>N$: In this case, $\tau<1$, and

$$\lim_{\xi\to-\infty}\frac{e^{-\tau\xi}}{\cosh\xi} = 0.$$

That means that we can make the same the approximation for the free energy that we made when we evaluated $G_\xi \ln(1+\eta_n^r)$. Therefore, we have

$$F^i \sim -TS^i - T\left[A + B\left(\frac{H}{T}\right)^2\right]\left(\frac{T}{T_0}\right)^{\tau}, \tag{3.28}$$

with A and B being constants O the order of unity, and we obtain

$$C^i \propto \left(\frac{T}{T_0}\right)^{2N/(N+f)}, \quad \chi^i \propto \frac{1}{T_0}\left(\frac{T}{T_0}\right)^{(N-f)/(N+f)}. \tag{3.29}$$

Needless to say, when $N=2$, we recover the multichannel results. As a matter of fact, the exponents depend only on the ratio $\gamma = f/N$.[5, 15–17]

Case $f=N$: Since $\tau=1$ in this case, we cannot extend the integral in Eq. (3.27) to $\xi\to-\infty$, and we have to restrict it to the interval $[\delta,\infty)$, where δ is a finite number of the order of one. Making use of $\int[dz/(1+e^{2z})] = z - \frac{1}{2}\ln(1+e^{2z})$ we have, for very low temperatures,

$$\Delta F^i \propto -\frac{T}{2\pi}\left(\frac{T}{T_0}\right)\int_{\delta-\ln T_0/T}^{\infty} d\xi \sum_{q=1}^{N} \frac{\left(\sin\pi\frac{N-q}{N}\right)(\alpha^q+\beta^q x_0^2)e^{-\xi}}{\cosh(\xi)+\cos\pi\frac{N-q}{N}} \propto -TS^i + \frac{T^2}{T_0}\frac{\ln T}{T_0}\left[A + B\left(\frac{H}{T}\right)^2\right].$$

Hence

$$C^i \propto -\frac{T}{T_0}\ln\frac{T}{T_0}, \quad \chi^i \propto -\frac{1}{T_0}\ln\frac{T}{T_0}. \tag{3.30}$$

Case $f<N$: In this region $1<\tau<2$. Consider the integral

$$\int_{\delta-\log T_0/T}^{\infty}\frac{e^{-(\tau-1)x}dx}{1+e^{2x}} = \frac{1}{\tau-1}\int_{\beta(T/T_0)^{\tau-1}}^{\infty}\frac{dy}{y^2(1+y^{2/(\tau-1)})}. \tag{3.31}$$

It is possible to find a primitive for $2/(\tau-1)$ integer; we have

$$\int \frac{dy}{y^2(1+y^{2/\tau-1})} = -\frac{1}{y} + \begin{cases} \frac{1}{2n}\sum_{k=1}^{n} \cos\frac{\pi(2n-1)(2k-1)}{2n} \ln\left(1-2y\cos\frac{\pi(2k-1)}{2n}+y^2\right) \\ \quad -\frac{1}{n}\sum_{k=1} \sin\frac{\pi(2k-1)(2n-1)}{2n} \arctan\left(\frac{y-\cos\frac{\pi(2k-1)}{2n}}{\sin\frac{\pi(2k-1)}{2n}}\right), & \frac{2}{\tau-1}=2n \\ \frac{\ln(1+y)}{2n+1} + \frac{1}{2n+1}\sum_{k=1}^{n} \cos\frac{\pi(2n)(2k-1)}{2n+1} \ln\left(1-2y\cos\frac{\pi(2k-1)}{2n+1}+y^2\right) \\ \quad -\frac{2}{2n+1}\sum_{k=1} \sin\frac{\pi(2k-1)(2n)}{2n+1} \arctan\left(\frac{y-\cos\frac{\pi(2k-1)}{2n+1}}{\sin\frac{\pi(2k-1)}{2n+1}}\right), & \frac{2}{\tau-1}=2n+1. \end{cases}$$

As $T\to 0$, the leading terms are of the form

$$\left(\frac{T}{T_0}\right)^{\tau-1} + \text{const.}$$

Hence

$$\Delta F^i \propto -\left[A+B\left(\frac{H}{T}\right)^2\right]\left[\frac{T^2}{T_0} - \text{conts. } T\left(\frac{T}{T_0}\right)^{\tau}\right].$$

Since $\tau>1$, the dominant term in ΔF^i is of order T^2. As for the specific heat and susceptibility, we have

$$C^i \propto \frac{T}{T_0} - A\left(\frac{T}{T_0}\right)^{2N/(N+f)}, \quad \chi^i \propto \frac{1}{T_0} - B\left(\frac{T}{T_0}\right)^{(N-f)/(N+f)}. \tag{3.32}$$

These results are valid for any $1<\tau<2$, as can be verified by numerical integration of Eq. (3.31), or by the numerical solution of the thermodynamic equations.

To summarize, there are three different kinds of behavior in the overscreened sector, depending on the value of the ratio $\gamma=f/N$. (i) When $\gamma>1$, both C^i/T and χ^i have power-law divergences as $T\to 0$. The behavior is similar to that of the multichannel Kondo model with $f>2$. Indeed, the exponents are the same, since they depend on γ only. (ii) For $\gamma=1$, there are logarithmic divergences as in the two-channel Kondo model. (iii) When $\gamma<1$, the values of C^i/T and χ^i at $T=0$ are finite. Actually, it can be deduced from the numerical analysis that these constants are the same as in the corresponding completely screened cases ($\mu=f$; as we will see later). However, the fixed point has non-Fermi-liquid behavior, as can be seen from the value of the residual entropy and from the subleading power-law terms.

One can relate the different kinds of behavior to the shape of the $n<f$ sector in Fig. 1, as can be seen in diagrams (3.19)–(3.21). The square diagram corresponds to $\gamma=1$, whereas the horizontal (vertical) one corresponds

D. Channel anisotropy

In this section we briefly consider the case when some of the couplings J_m are different. From the study of the analogous problem in the multichannel Kondo model,[18] we conclude that up to f different energy scales will appear in the problem depending on the pattern of symmetry breaking. The novelty here is that there might be a situation where $\gamma>1$ for an intermediate regime of temperatures, whereas for very low temperatures the behavior is characterized by an effective γ smaller than 1.

Consider a system where the flavor symmetry is such that p energy scales $T_1<T_2<\cdots<T_p$ are generated. Each scale T_j is related to a driving term at the level $n=m_j$ in the TBA equations (3.7). We will assume for simplicity, that $m_1<m_2<\cdots<m_p=f$. If the largest flavor symmetry possible is SU(f), there will always be a driving term at the level $n=f$.

Then, when the temperature is below any T_j, the thermodynamic properties are given by Eqs. (3.16) and (3.29), where $\gamma=f/N$ is replaced by $\gamma_{eff}=m_1/N$. As the temperature is increased, the behavior of the system when $T_{j-1}<T<T_j$ corresponds to $\gamma_{eff}=m_j/N$. Indeed, the value to the impurity contribution to the entropy will be close to $\mathcal{S}^i(m_j,N)$.

Flavor anisotropy is a relevant perturbation of the isotropic Hamiltonian. In general, the system will flow away from the fixed point characterized by f, and N to a new fixed point characterized by $m_1<f$, and N. From Eq. (3.16), we see that $\mathcal{S}^i$ is reduced in such flow [$\mathcal{S}^i(f,N)$ is monotonous in both f and N]. It is worth noticing that, once $m_1<N$, χ^i and C^i/T become constant as $T\to 0$.

The system of TBA equations are represented diagrammatically in Fig. 3. Depending on the pattern of symmetry breaking, driving terms appear at different values of n. There are always driving terms for $n=f$. The properties at temperatures between two different scales are related to the corresponding overscreened part of the diagram. Notice that channel anisotropy may have the effect of changing the shape in the overscreened area from something similar to Eq. (3.21) to diagrams like Eqs. (3.20), and (3.21), but not the other way around.

E. Impurity in a higher-dimensional representation

Finally, we study a generalization of the model in which the impurity behavior is that of an object in a rank μ repre-

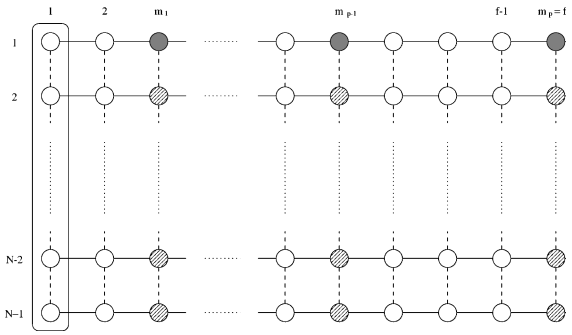

FIG. 3. Same as Fig. 1, but now the interaction with the impurity breaks the flavor symmetry from SU(f) down to $\Pi_{j=1}^{p}\mathrm{SU}(m_j-m_{j-1})$, with $m_j^p=f$ and $m_0=0$.

sentation of SU(N). In the SU(2) case it corresponds to an impurity with spin S. Following Ref. 19 and the same formulation that we followed for the fundamental representation, we find the following set of effective Bethe ansatz equations

$$e^{ifp_\delta L}=\prod_{\gamma=1}^{M^1}\frac{\chi_\gamma^1-1+if\frac{c}{2}}{\chi_\gamma^1-1-if\frac{c}{2}},$$

$$-\prod_{\beta=1}^{M^r}\frac{\chi_\gamma^r-\chi_\beta^r+ic}{\chi_\gamma^r-\chi_\beta^r-ic}=\prod_{t=r\pm1}\prod_{\beta=1}^{M^t}\frac{\chi_\gamma^r-\chi_\beta^t+i\frac{c}{2}}{\chi_\gamma^r-\chi_\beta^t-i\frac{c}{2}};$$

$$r=2,\ldots,N-1,$$

$$-\prod_{\beta=1}^{M^1}\frac{\chi_\gamma^1-\chi_\beta^1+ic}{\chi_\gamma^1-\chi_\beta^1-ic}=\frac{\chi_\gamma^1+i\mu\frac{c}{2}}{\chi_\gamma^1-i\mu\frac{c}{2}}\prod_{\delta=1}^{N^e/f}\frac{\chi_\gamma^1-1+if\frac{c}{2}}{\chi_\gamma^1-1-if\frac{c}{2}}\times\prod_{\beta=1}^{M^2}\frac{\chi_\gamma^1-\chi_\beta^2+i\frac{c}{2}}{\chi_\gamma^1-\chi_\beta^2-i\frac{c}{2}}.$$

The impurity contribution to the free energy is

$$F^i=-T\sum_n\int_{-\infty}^{\infty}B_{n,\mu}\ln[1+(\eta_n^1)^{-1}].$$

As in the $\mu=1$, a series of transformations allow us to rewrite the free energy as

$$F^i=\sum_{q=1}^{N-1}\int_{-\infty}^{\infty}d\chi G_N^{1,q}(\chi)g_\mu^q(\chi)-T\times\sum_{q=1}^{N-1}\int_{-\infty}^{\infty}d\chi G_N^{1,q}(\chi)\ln(1+\eta_\mu^q),$$

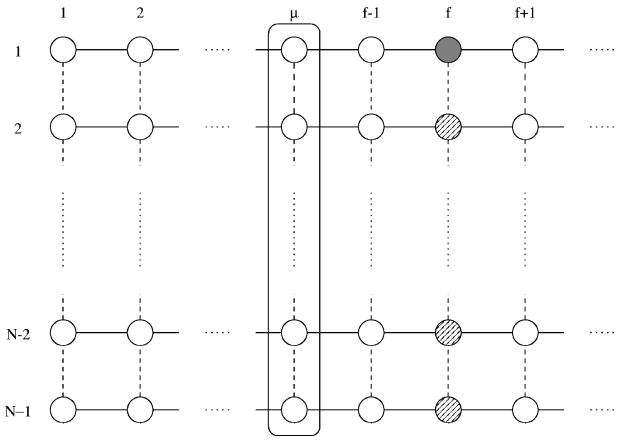

FIG. 4. Same as Fig. 1, but now the impurity contribution to the free energy involves the set η_μ^q, where μ is the rank.

where the first term corresponds to the impurity contribution to the ground state. At finite temperatures we are only interested in the second term, which in the scaling limit can be written as

$$F^i=-\frac{T}{2\pi}\sum_{q=1}^{N}\int_{-\infty}^{\infty}d\xi\frac{\left(\sin\pi\frac{N-q}{N}\right)\ln[1+\eta_\mu^q(\xi)]}{\cosh\left(\xi-\ln\frac{T_0}{T}\right)+\cos\pi\frac{N-q}{N}}.\tag{3.33}$$

The evaluation of F^i involves the functions η_μ^r, (see Fig. 4). The different scenarios possible are very similar to those of the multichannel Kondo model. As long as $\mu<f$, the impurity remains overscreened and the temperature exponents are the same as for the $\mu=1$ case. In this case, the residual entropy is

$$\mathcal{S}_{T=0}^i=\ln\frac{\prod_{r=1}^{\mu+N-1}\sin\frac{\pi r}{f+N}}{\prod_{r=1}^{\mu}\sin\frac{\pi r}{f+N}\prod_{r=1}^{N-1}\sin\frac{\pi r}{f+N}}\tag{3.34}$$

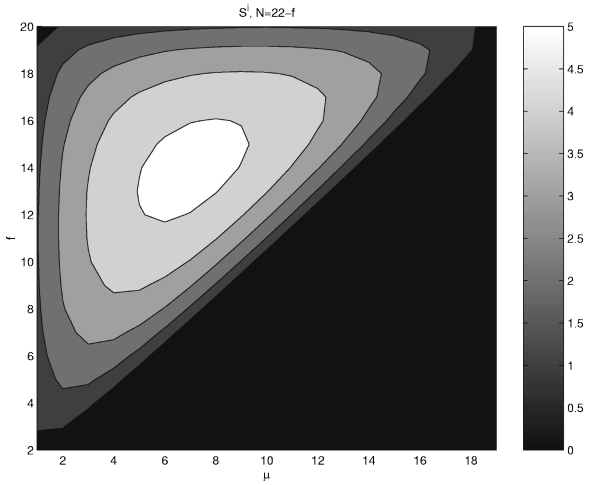

FIG. 5. Overscreening residual entropy, $S_{\mu<f}^i$, for an impurity in a totally symmetric representation μ of SU(N), for $N+f=22$. The lower triangular region (in black) is unphysical.

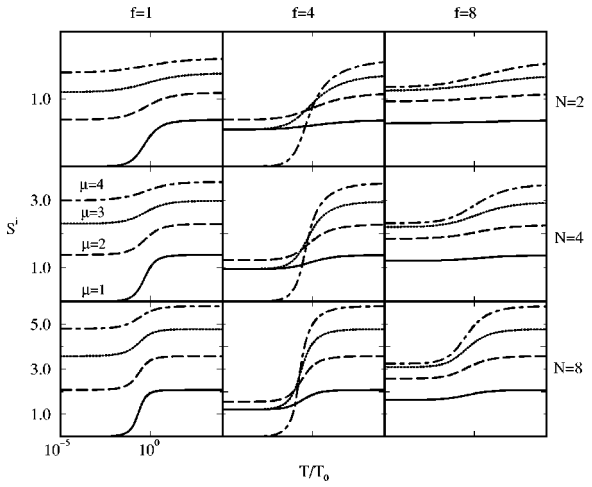

FIG. 6. Impurity contribution to the entropy as a function of T, for different values of N, f, and impurity spin μ. Notice that different scales are used for the different N.

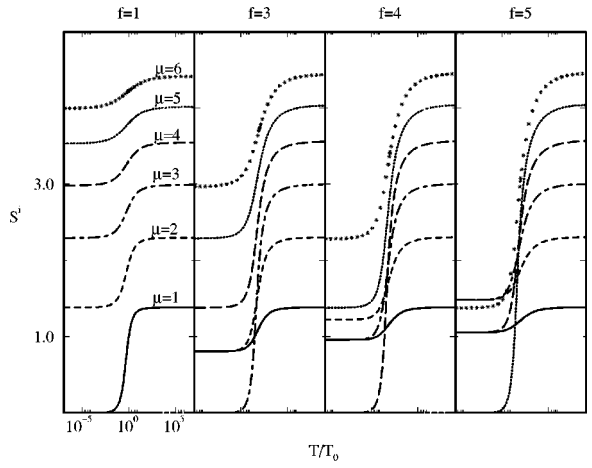

FIG. 7. $\mathcal{S}^i$ vs T for $N=4$, $f=1$, 3, 4, and 5, and $\mu=1,\ldots,6$.

[Notice that when $N=2$ this reduces to the multichannel result $\ln(\sin[\pi(2S+1)/(f+2)]/\sin[\pi/(f+2)])$]. Furthermore, it can be easily shown that $\mathcal{S}^i_\mu=\mathcal{S}^i_{f-\mu}$.

We have plotted $\mathcal{S}^i$ in Fig. 5, for fixed $N+f=22$, and several values of $\gamma=f/N$ and μ. Only the region $\mu<f$ is physical in the figure, since these are results for the overscreened case. We can see that for fixed (even) f, the largest value of the entropy corresponds to $\mu=f/2$. Also, for fixed μ, the entropy is the largest around $\gamma\sim 1$, and decreases as γ moves away from 1.

If $\mu=f$ the impurity becomes completely screened: χ^i and C^i/T become constant, and there is no residual entropy. Finally, if $\mu>f$, the impurity is underscreened. The dominant contribution to the free energy from the spin sector is of the form

$$F^i=-T\ln\frac{\prod_{r=1}^{\mu-f+N-1}\sinh r\frac{H}{T}}{\prod_{r=1}^{\nu-f}\sinh r\frac{H}{T}\prod_{r=1}^{N-1}\sinh r\frac{H}{T}}.$$

When $H=0$, the residual entropy is

$$\mathcal{S}^i=\ln\frac{(\mu-f+N-1)!}{(\mu-f)!(N-1)!}=\ln\binom{\mu-f+N-1}{N-1}.$$

[For $N=2$, the residual entropy is $\ln\binom{\mu-f+1}{1}=\ln(\mu-f+1)$.]

IV. NUMERICAL ANALYSIS

A. Procedure

We have solved the TBA equations by iteration, using a procedure inspired by the work of Rajan.[20] For the levels $n\neq f$, which do not have a driving term (see Fig. 4), we have used Eqs. (3.2) and (3.3) as the starting point, since it is more convenient to use the kernel $G(\xi)$. We have dealt with the equations that have a driving term by introducing two sets of auxiliary functions,[12]

$$h^r(\xi)=G_\xi[\ln(1+\eta^n_{f+1})+\ln(1+\eta^n_{f-1})],$$

$$Q^r(\xi)=G_\xi[Q^{r+1}(\xi')+Q^{r-1}(\xi')]-h^r(\xi),$$

so that

$$\ln\,\eta^r_f=-\frac{2}{f}e^\xi\sin\left(\frac{\pi r}{N}\right)+\ln(1+\eta^r_f)+Q^r.$$

We have introduced a cutoff A in the integrals involved, taken $\ln(1+\eta^r_n)$ to be constant for $|\xi|>A$, and evaluated the integrals in those intervals analytically. For $|\xi|<A$ we have replaced the integral with a sum using a Gaussian quadrature rule.[21]

The results that we present in this work correspond to zero magnetic field, which means that $x_0=H/T=0$, and the functions η^r_n depend on ξ only. Thus the task of obtaining thermodynamic properties is greatly simplified. First of all, the impurity contribution is given by Eq. (3.6)

$$F^i=-\frac{T}{2\pi}\sum_{q=1}^{N}\int_{-\infty}^{\infty}d\xi\,\frac{\left(\sin\,\pi\frac{N-q}{N}\right)\ln[1+\eta^q_\mu(\xi)]}{\cosh\left(\xi-\ln\frac{T_0}{T}\right)+\cos\,\pi\frac{N-q}{N}},$$

with η^r_n independent of T. The entropy and specific heat are obtained by taking derivatives of F^i with respect to the temperature, which can be done analytically when $x_0=0$, and then performing the integration numerically.

In order to calculate the susceptibility at zero magnetic field, χ^i, we derived a second set of TBA equations for the functions

$$E^r_n(\xi)\equiv\left.\frac{\partial^2\eta^r_n(\xi)}{\partial x_0^2}\right|_{x_0=0},$$

following Degranges.[22] This system is solved as the previous one, and the magnetic susceptibility is given by

$$\chi^i|_{x_0=0}=\frac{\partial^2 F^i}{\partial x_0^2}=-\frac{T}{2\pi}\sum_{q=1}^{N}\int_{-\infty}^{\infty}d\xi\,\frac{\left(\sin\,\pi\frac{N-q}{N}\right)E_\mu^q(\xi)}{\cosh\left(\xi-\ln\frac{T_0}{T}\right)+\cos\,\pi\frac{N-q}{N}}.$$

B. Results

1. Entropy

We start by discussing the impurity contribution to the entropy, $\mathcal{S}^i$. In Fig. 6, we have plotted $\mathcal{S}^i$ as a function of T, for different values of N, f, and impurity spin μ. The horizontal axis is on a logarithmic scale. The vertical axes have different scales for the different N. The first thing to notice is the crossover around $T\sim T_0$. For $T\gg T_0$, $\mathcal{S}^i$ is that of a free spin characterized by μ and N. When $H=0$,

$$\mathcal{S}^i=\ln\binom{\mu+N-1}{N-1}.$$

Below the crossover region one can see the quenching of the degrees of freedom due to the interaction in the decrease of the value of the entropy. The qualitative behavior of $\mathcal{S}^i$ in the region $T\ll T_0$ depends only on the relation between μ and f. When $f=\mu$, there is complete screening, and $\mathcal{S}^i=0$, as can be seen in the curves $\mu=f=1$ and $\mu=f=4$. For $\mu>f$, the impurity is not completely screened, and there is effectively a leftover free spin $\mu-f$, as can be seen in Fig. 6 for $f=1$. There, the $T\ll T_0$ entropy for $\mu<f$ corresponds to the $T\gg T_0$ entropy for $\mu-1$. Finally, when $\mu<f$, overscreening takes place: even though there are enough electrons to form a singlet with the impurity, the low-temperature behavior is characterized by an object with complex internal structure, and an anomalous $\mathcal{S}^i$. Such behavior can be seen in the curves $\mu=2$ and $\mu=3$ for $f=4$, and in all the curves for $f=8$. Notice that for $\mu=1$ and $\mu=f-1$, the curves converge to the same value, as we had already seen in the asymptotic analysis. Furthermore, the overscreened fixed point has an anomalous residual entropy irrespective of the value of N, indicating its non-Fermi-liquid nature.

A more detailed picture of the behavior of $\mathcal{S}^i$ for $N=4$ is displayed in Fig. 7. It is worth noticing that in the underscreened cases, the effective spin is $\mu-f$. Also, there might be situations where the residual entropy of the overscreened case is larger than that of the underscreened case. Such is the case for $f=5$, $\mu=3$ and 4, as compared to $\mu=6$.

2. Specific heat

Next, we compute the contribution to the specific heat. Results for different values of the parameters are shown in Fig. 8. The largest maximum of C_V^i corresponds to $\mu=f$. Also, the size of the curve grows with N.

We have also evaluated the subleading contribution to the linear coefficient of the specific heat, $\gamma^i=C_V^i/T$ for $f=2\mu=2$, $N>f$, and have plotted it in Fig. 9. The points fit power-law curves with exponents $(N-f)/(N+f)$, derived previously [see Eqs. (3.29), (3.30), and (3.32)]. This is another clear indication that for $N>f$, the overscreened cases are not Fermi-liquid fixed points.

3. Magnetic susceptibility

Next, we have studied $T\chi^i$ for different values of the parameters, and plotted the results in Fig. 10. As with the entropy, the qualitative behavior depends only on the values of μ and f. The difference in behavior between underscreened and overscreened cases becomes more clear here: whereas the magnetic moment is partially quenched in the former

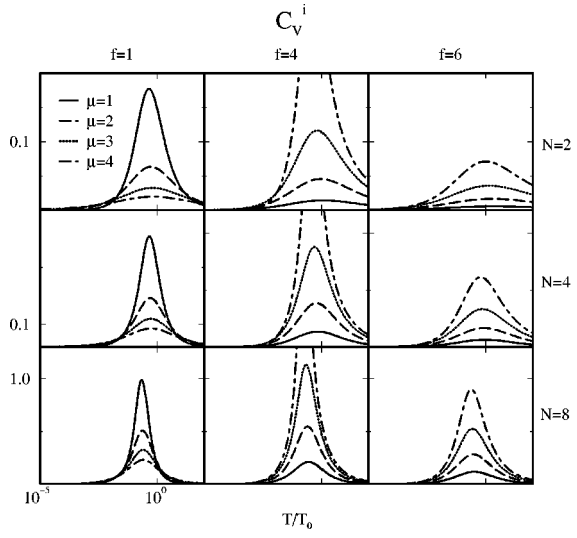

FIG. 8. Impurity contribution to the specific heat, C_V^i, for different values of N, f, and μ.

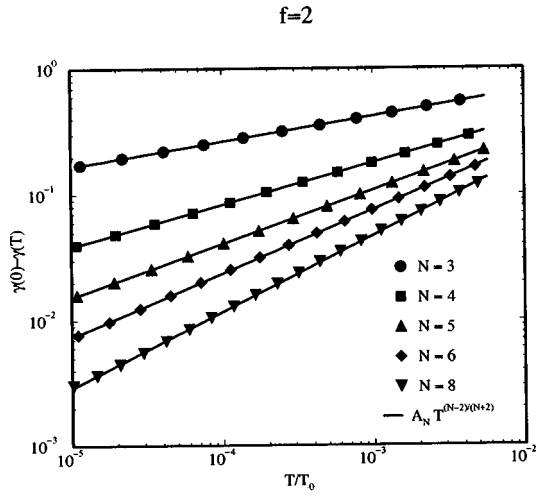

FIG. 9. Subleading contribution to $\gamma(T)=C_V^i/T$, for $f=2$, $\mu=1$, and $N>f$ vs T on a log-log graph. The symbols correspond to the numerical calculation. The lines correspond to power-law fits with exponents $(N-2)/(N+2)$.

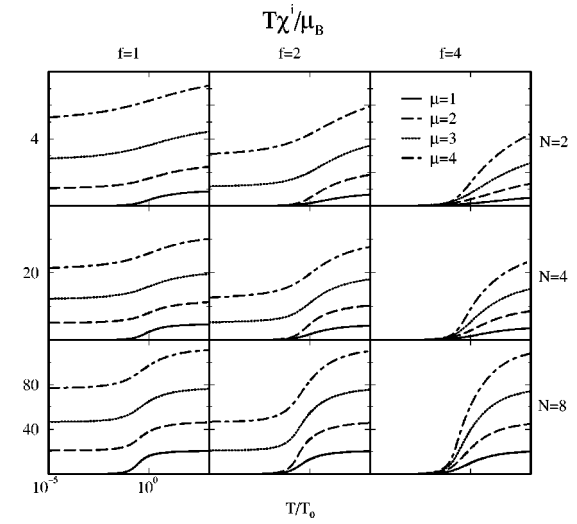

FIG. 10. $T\chi^i$ vs T, for different values of f, N, and μ.

case, the overscreened case is characterized by a totally quenched moment, even though there is a nonzero residual entropy. This can be seen in Fig. 10 for the curves with $f=1$ and 4.

The magnetic susceptibility is plotted in Fig. 11. The curves with $f=\mu$ have a constant χ^i at low T, and for $N>2$ they have a maxima near $T\sim T_0$. This is a special feature of the completely screened case. We see that in the overscreened case with $N>f$, the susceptibility tends to a finite value as $T\to 0$, while it diverges when $N\leqslant f$. When $N=f$, the divergence is logarithmic, whereas it is a power law for $N<f$, with an exponent $\beta>-1$. The largest divergence corresponds to the underscreened case with $1/T$ behavior. All these results coincide with those of the previous analytic study [Eqs. (3.29), (3.30), and (3.32)]. (Also see Fig. 12).

In Fig. 13 we show χ^i for different values of N for the cases $\mu=f=1$ and $\mu=f=4$. We have rescaled the curves dividing by $\chi^i(0)$. It is quite apparent that the behavior is the same in both cases.

In Fig. 14 we consider $N=8$, $f=7$ and $\mu=1,\ldots,7$. Even though $\chi^i(0)$ is finite, it is clear that the behavior of the

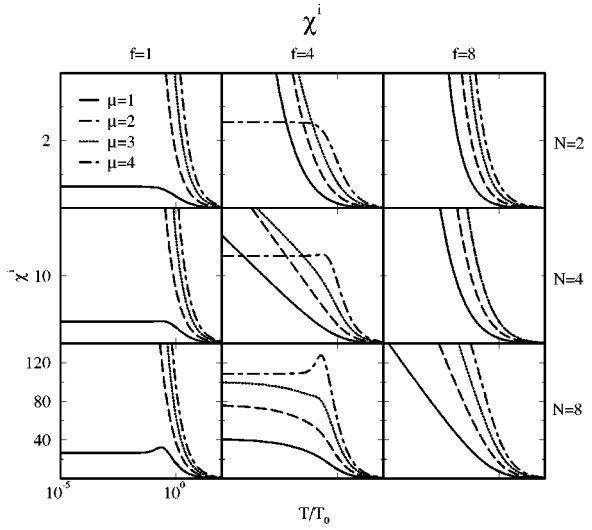

FIG. 11. Impurity contribution to the magnetic susceptibility, χ^i vs T, for different values of f, N, and μ.

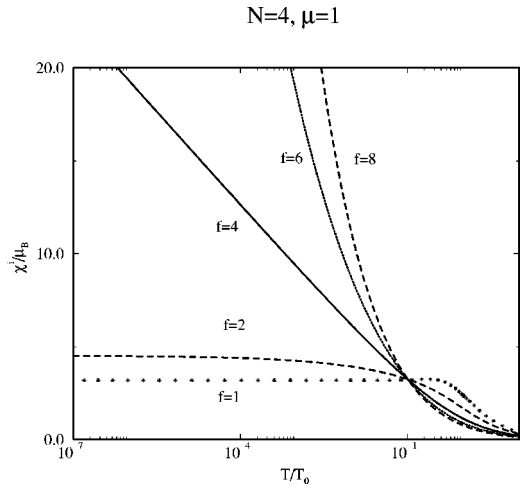

FIG. 12. χ^i vs T for $N=4$, $\mu=1$, and $f=1$, 2, 4, 6, and 8.

overscreened case is quite different from that of the completely screened case, and that the subleading terms have an important contribution below the crossover temperature.

We can also see the power-law behavior of the subleading term of χ^i in Fig. 15. The values for the exponents agree with the values obtained analytically, i.e., $(N-f)/(N+f)$.

4. Wilson ratio

We have calculated the Wilson ratio, defined as

$$R\equiv\frac{\pi^2 k_B^2}{(N^2-1)\mu_B^2}\frac{T\chi^i}{C_V^i}. \tag{4.1}$$

The quantity R has a well-defined meaning only for $T=0$. However, in Fig. 16 we have plotted the quantity $R(T)$, to show the difference between the $N<f$ and the $N>f$ sectors. In the former case, $(N=2,\ f>1)$, the value for the overscreened case is much larger than the value of the completely screened case (notice the difference in vertical scales), whereas in the latter case $(N=8)$, the curves converge to the completely screened value. Notice that for $N=4$ there is a change in behavior as we go from $f<N$ to $f>N$.

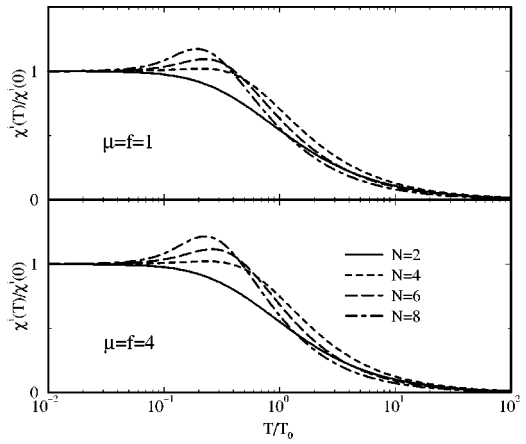

FIG. 13. $\chi^i(T)/\chi^i(0)$ vs T for different values of N, in two completely screened cases $\mu=f=1$ and $\mu=f=4$.

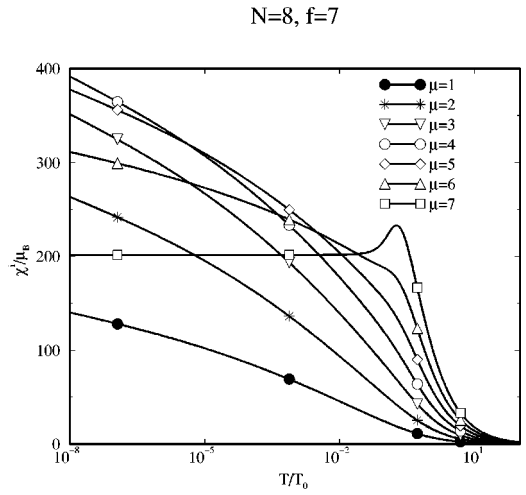

FIG. 14. χ^i vs T for $N=8$, $f=7$, and $\mu=1,\ldots,7$.

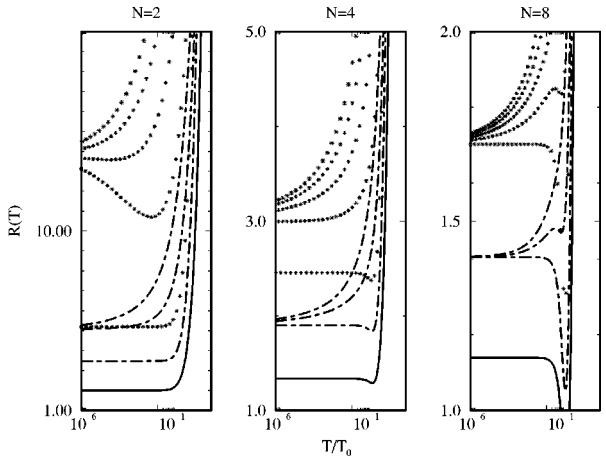

FIG. 16. $R(T)$ as a function of temperature for $N=2,4,8$, $\mu=1,\ldots,f$, and $f=1$, 3, and 5.

Next we plot the values of R for completely screened cases, $\mu=f$ (Fig. 17). We see that the values obtained fit the function

$$R=\frac{N(N+f)}{N^2-1}. \tag{4.2}$$

We have also obtained values of R for the overscreened case ($\mu<f$) in Fig. 18. There are clear differences between the $f<N$ and the $f>N$ cases, as we have already pointed out. For $f<N$, the value of R coincides with the value for $\mu=f$, and agree with Eq. (4.2). The dominant contribution to R comes from the constant terms in χ^i and C_V^i/T. For $f>N$, R contains mainly the coefficients of the divergent parts, and have a different functional behavior.

5. Channel anisotropy

We end the discussion of the numerical results by showing an example of channel anisotropy. We have taken the case $N=3$, with original flavor symmetry SU(6), broken down to SU(4)×SU(2) (Fig. 19) Two scales appear in this problem: T_6, and T_4. Accordingly, the TBA equations have driving terms at $n=4$ and 6. We have chosen very small anisotropy, $T_4/T_6=10^{-6}$. In Fig. 20, we have plotted the entropy for different values of μ. There are three different regions: When $T\gg T_6$, the impurity behaves like a free moment. Around $T\sim T_6$ there is a crossover to an overscreened region (when $\mu<6$), characterized by an SU(6) flavor symmetry. The pairs of curves $(\mu,6-\mu)$ merge. Notice also that $\mu=6$ is completely screened. There is a second crossover around $T\sim T_4$ to a region characterized by SU(4) flavor symmetry for $\mu<4$ and by SU(2) flavor symmetry for $4<\mu<6$. Only the curves for $\mu=1$ and $\mu=(4-1)=3$ coincide now. Also, the value of the residual entropy for $\mu=1$, is that of an effective $\mu=1$ in an SU(3)×SU(2) model. The entropy for $\mu=4$ goes to 0 with T, since the system becomes screened for $T\ll T_4$.

Finally, we have plotted C_V^i/T for several μ in Fig. 21. When $T_4\ll T\ll T_6$, the behavior of the system is characterized by $f=6$: increasing value of C_V^i/T for $\mu<6$, constant behavior for the screened case, $\mu=6$. Near T_4 the curves for $\mu<6$ have a similar behavior as those for free moments (however, such behavior is not found in the curves for the magnetic susceptibility). We can see three different behaviors in the region $T\ll T_4$. For $\mu=1$ the curve diverges with

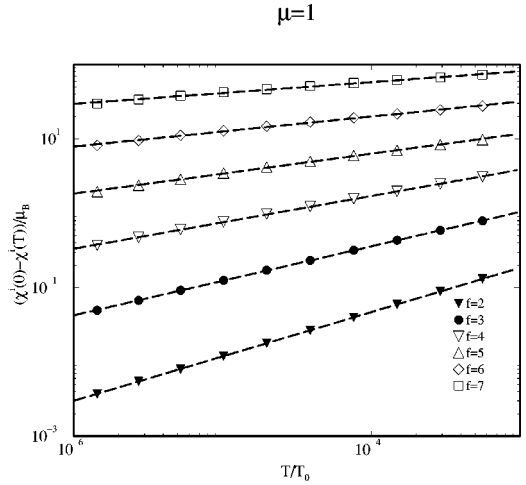

FIG. 15. Subleading T dependence of χ^i for $N=8$, $f=2,\ldots,7$, and $\mu=1$. The lines correspond to power-law fits.

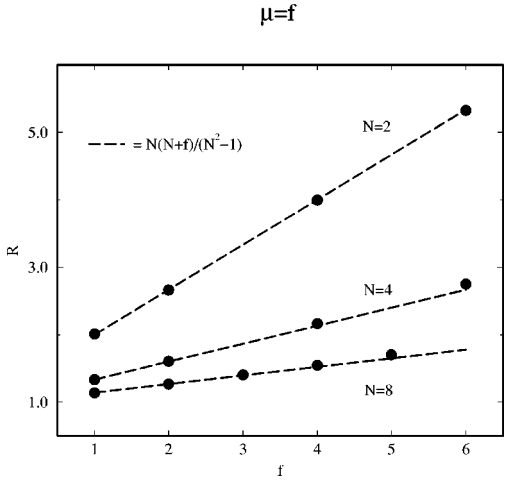

FIG. 17. Wilson ratio R for $\mu=f$. The points have been obtained from the numerical solution. The lines correspond to fits with the function $N(N+f)/(N^2-1)$.

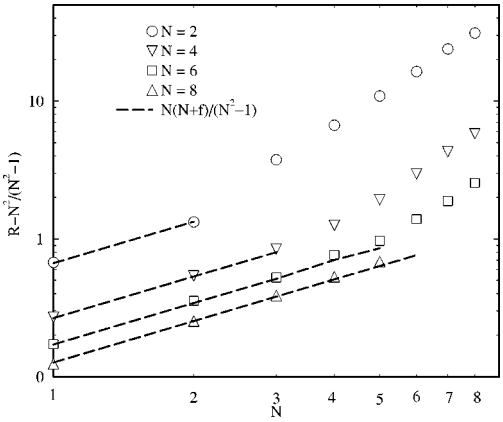

FIG. 18. Wilson ratio R for $\mu<f$. See the caption in Fig. 17.

a power law, as one would expect for $f_{eff}=4>N=3$. The curve for $\mu=4$ is flat, since the impurity is screened. Finally, for $\mu=5$, the curve increases slowly, converging to a constant value, as one would expect from an effective $f_{eff}=2<N=3$.

V. PHYSICAL REALIZATIONS OF THE SU(N)×SU(F) MODEL

In the present section we shall concentrate on the possible physical realizations and applications of the SU(N)×SU(f) Coqblin-Schrieffer model. In Secs. V A, V B, and V C, we analyze the so called N-level system (NLS) model, a generalization of the two-level system model,[2] by means of a systematic $1/f$ expansion. In this context the flavor degeneracy is associated with the physical spin of the electron. First we establish a mapping of the NLS model to the multichannel Coqblin-Schrieffer model (MCCS model) by analyzing the low-energy fixed point of its scaling equations. While our procedure gives a systematic expansion only for the case $f>N$, we shall argue that the same mapping should apply for the cases $f\leqslant N$.

In the limit $f>N$ we are able to determine the full operator content of the fixed point. This enables us to calculate the scaling of the different physical quantities at low temperatures in Sec. V C. As we shall see, there are some subtle differences between the two models, and while most of the physical quantities show the same dependence, the scaling of the specific heat may be different. The origin of these differences will be discussed in detail. Finally, based on the results of Secs. V A–V C, in Sec. V D we discuss some physical systems providing possible candidates for the realization of the MCCS model.

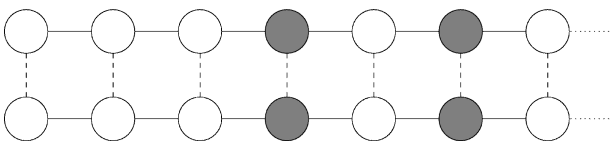

FIG. 19. Diagrammatic representation of the TBA equations for a system with $N=3$, and flavor symmetry SU(6) broken down to SU(4)×SU(2). Two driving terms appear at $n=4$ and 6.

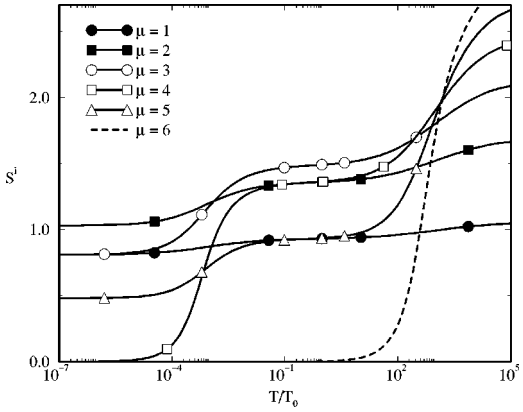

FIG. 20. Entropy vs T, for $\mu=1,\ldots,6$.

A. N-level system model and its low-energy fixed point

The NLS model has been constructed as a generalization of the two-level system model[2,23] to describe the tunneling of a heavy particle among N not necessarily equivalent positions labeled by $a=\{1,..,N\}$, and strongly coupled to the conduction electrons. At low temperatures the motion of the heavy particle can be described by the effective Hamiltonian

$$H_{\rm hp}=\sum_{a,b=1}^{N}\chi_a^+\Delta^{ab}\chi_b\,, \tag{5.1}$$

where χ_a^+ creates a pseudofermion[24] corresponding to the heavy particle site a, and Δ^{ab} is the tunneling amplitude between positions a and b. If no external stress is present then the diagonal part of Δ^{ab} vanishes: $\Delta^{aa}=0$ ($a=1,...,N$), when the N positions are equivalent due to the symmetry of the NLS. The electronic part of the Hamiltonian and the coupling of the heavy particle to the conduction electrons take the general form

$$H_{\rm el}=\sum_{\epsilon nm}\epsilon c_{\epsilon nm}^+c_{\epsilon nm}\,,$$

$$H_{e\text{-hp}}=\sum_{\substack{a,b,n,n'\\ \epsilon,\epsilon',m}}c_{\epsilon nm}^+\chi_a^+V_{nn'}^{ab}\chi_b c_{\epsilon' n' m}\,, \tag{5.2}$$

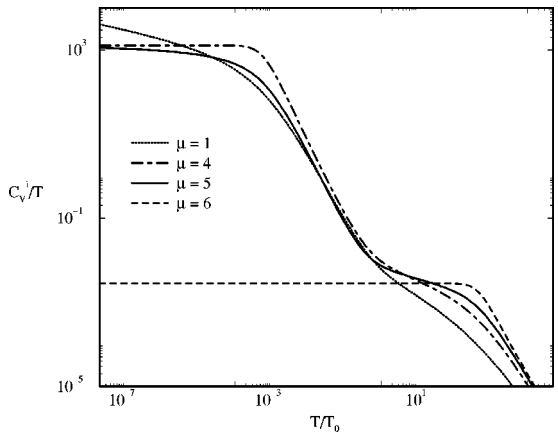

FIG. 21. C_V^i/T vs T, for $\mu=1$, 4, 5, and 6.

where the operators $c^{+}_{\epsilon nm}$ create conduction electrons with energy ϵ, orbital quantum number[2] ($\sim$ angular momentum) $n=1,2,...,\infty$, and spin m. For the sake of simplicity the electronic density of states $\varrho(\epsilon)$ is assumed to be constant ϱ_0, between the high- and low-energy cutoffs, D and $-D$, independently of the flavor and orbital quantum numbers. While in the physical case only $m=\pm$ is possible corresponding to the two different spin directions, in the following for technical reasons we assume that the electron spin m can take f different values: $m=1,...,f$.

This model has a structure similar to Eq. (2.1) but there are some important differences. The ''spin index'' $a'=1,...,N$ of the impurity in Eq. (2.1) is now replaced by the ''site index'' $a=1,...,N$ of the heavy particle. Moreover, in the NLS case the orbital index n [replacing the spin index $a=1,...,N$ of the conduction electrons in the SU(N) $\times$SU(f) model] now ranges from 1 to infinity, since the conduction electrons may have any orbital momentum. Furthermore, the couplings are *very anisotropic* in orbital indices and no SU(N) symmetry is present at this level. Finally, in the NLS model the scattering is diagonal in the real spin index m, which plays now the same role as the flavor in Eq. (2.1).

The diagonal couplings, $V^{aa}_{nn'}$ describe simple potential scattering of the conduction electrons by the heavy particle sitting in position a. On the other hand, the off-diagonal matrix elements $V^{ab}_{nn'}$, with $a\neq b$, correspond to the so-called ''assisted tunneling'' processes. Here the heavy particle is tunneling from one site to another while a conduction electron is scattered by it. The combination of these two processes leads ultimately to the generation of an orbital Kondo effect and a strongly correlated ground state.[2,5]

In the following we shall carry out a large f analysis to determine the low-energy fixed point of the NLS model. While our procedure is strictly valid only in the case $f>N$, in the end of the subsection we shall argue that our results are very general, and that they should apply even for the cases $f\leqslant N$.

To carry out a $1/f$ analysis of the NLS model, as a next step, we construct the next to leading logarithmic scaling equations using a generalized multiplicative renormalization group technique.[5] As discussed in Refs. 1, 16, 17, and 25, the leading logarithmic equations give the leading term in a systematic $1/f$ expansion and become exact in the $f\to\infty$ limit. In the multiplicative renormalization-group method, one exploits the existence of a nontrivial transformation in the space of the Hamiltonians, $D\to D'$, $V^{ab}_{nn'}\to V'^{ab}_{nn'}$ and $\Delta^{ab}\to\Delta'^{ab}$, that leaves the pseudofermion Green's function $\mathcal{G}^{ab}$ and the pseudofermion-conduction electron vertex function $\Gamma^{ab}_{nn'}(\omega)$ invariant:

$$\mathcal{G}(\omega,V',\Delta',D')=A\mathcal{G}(\omega,V,\Delta,D)A^{+},$$
$$\Gamma(\omega,V',\Delta',D')=[A^{+}]^{-1}\Gamma(\omega,V,\Delta,D)A^{-1}. \tag{5.3}$$

In these equations A denotes an $N\times N$ matrix independent of the energy variables ω and T, and acting in the site indices: $A=A^{ab}(V',\Delta',D'/D)$. By means of the transformation Eq. (5.3), one can generate effective Hamiltonians that describe the system's behavior below the energy scale D'. The generated effective Hamiltonians usually (in a renormalizable theory) turn out to be much simpler than the original one.

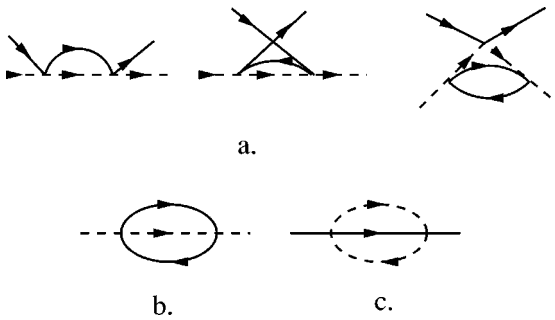

FIG. 22. The leading logarithmic vertex and self-energy diagrams generating the next-to-leading logarithmic scaling equations. Continuous and dashed lines represent the conduction electron and pseudofermion Green's functions.

To make use of the invariance property Eq. (5.3) one first has to construct the lowest-order vertex and pseudofermion self-energy corrections[2] arising from the diagrams in Figs. 22(a) and 22(b),

$$\Sigma^{ab}=-f\,\ln\frac{D}{\omega}\,(\delta^{ab}\omega\,\mathrm{tr}\{\underline{v}^{cd}\underline{v}^{dc}\}-\mathrm{tr}\{\underline{v}^{ac}\Delta^{cd}\underline{v}^{db}\}),$$
$$\varrho_0\underline{\Gamma}^{ab}=\underline{v}^{ab}-\ln\frac{D}{\omega}\,([\underline{v}^{ac},\underline{v}^{cb}]-f\,\mathrm{tr}\{\underline{v}^{ac}\underline{v}^{db}\}\underline{v}^{cd}), \tag{5.4}$$

where ϱ_0 is the density of states at the Fermi level, and a matrix notation has been introduced for the dimensionless couplings $\varrho_0\,V^{ab}_{nn'}\to\underline{v}^{ab}$. The symbol [,] stands for the commutator, the trace operator tr$\{\cdots\}$ is acting in the electronic indices, and a summation must be carried out over repeated indices. Then, substituting Eq. (5.4) into Eq. (5.3), and reducing the bandwidth D by an infinitesimal amount, one can deduce the infinitesimal renormalization-group transformations for the couplings:

$$\frac{d\Delta^{ab}}{dx}=-\frac{1}{2}f[\mathrm{tr}\{\underline{v}^{ac}\underline{v}^{cd}\}\Delta^{db}+\Delta^{ac}\mathrm{tr}\{\underline{v}^{cd}\underline{v}^{db}\}-2\mathrm{tr}\{\underline{v}^{ac}\Delta^{cd}\underline{v}^{db}\}], \tag{5.5}$$

$$\frac{d\underline{v}^{ab}}{dx}=-[\underline{v}^{ac},\underline{v}^{cb}]+\frac{1}{2}\,f(2\mathrm{tr}\{\underline{v}^{ac}\underline{v}^{db}\}\underline{v}^{cd}-\mathrm{tr}\{\underline{v}^{ac}\underline{v}^{cd}\}\underline{v}^{db}-\underline{v}^{ac}\mathrm{tr}\{\underline{v}^{cd}\underline{v}^{db}\}), \tag{5.6}$$

where the dimensionless scaling variable $x=\ln(D_0/D)$ has been introduced, D_0 being the initial (real) bandwidth cutoff of the model.

These scaling equations have to be solved with the boundary condition that the couplings are equal to their bare values at $x=0$, and they lose their validity if the reduced bandwidth D becomes smaller than any small-energy scale present: T, ω, or Δ. Note that, up to the next to leading logarithmic order, the splittings Δ^{ab} do not occur in Eq. (5.6) explicitly, and they provide only a low-energy cutoff for the scaling. To be explicit, there is an energy scale $D^*=T^*$ that we call the *freezing temperature*, where the renormalized splitting becomes of the same order of magnitude as the reduced band-

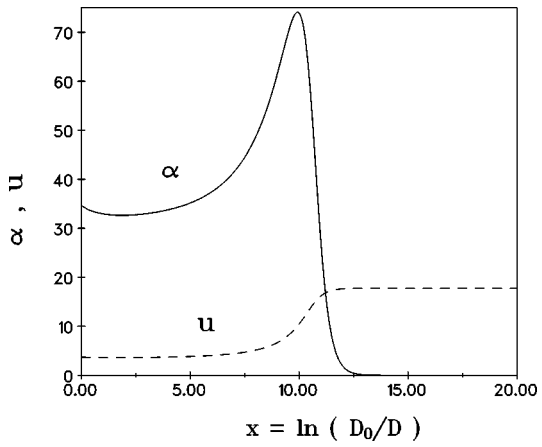

FIG. 23. Scaling of the norm of the dimensionless couplings, $u=\Sigma\|v^{ab}\|$ (dashed line), and of the algebra coefficient α (continuous line) for a six-state system with $f=2$.

width: $\Delta^{ab}(D^*)\sim D^*$. Below this energy scale the orbital motion of the NLS is usually frozen out (see the discussion in the end of this section), and the couplings may be replaced by their values at T^*.

For the moment let us forget about Eq. (5.5) and concentrate on the scaling of the $\underline{v}^{ab}$'s, Eq. (5.6). This equation cannot be solved generally, but one can convince oneself very easily that if the assisted tunneling matrix elements $\underline{v}^{ab}$ $(a\neq b)$ do not vanish, then the electron-NLS couplings start to increase and lead to a Kondo effect.[2,17] The scaling of the norm of the couplings, $\Sigma_{a,b}\|\underline{v}^{ab}\|$ is shown in Fig. 23 for a symmetrical six-state system, where the coupling constants have been estimated using similar methods as in Ref. 2. As one can see, a Kondo effect occurs around the Kondo scale $T_K\sim D_0\ e^{-x_c}\sim 10K$, where $x_c=\ln(D_0/T_K)$ denotes the value of the scaling parameter at which the crossover from weak to strong coupling occurs. Our numerical investigations for various model parameters and different values of N show that the structure of the stable low-temperature fixed point the couplings scale to is *independent* of the initial couplings, and only depends on the value of N if no some very restrictive symmetry is assumed for the $\underline{v}^{ab}$'s.

In what follows we shall show that this stable low-energy fixed point of Eq. (5.6) has in principle the structure of the defining representation of the SU(N) Lie algebra. To be precise we first observe that the operators $\mathcal{O}^a\sim\delta^{ab}\Sigma_c\underline{v}^{cc}$ are invariant under scaling. Therefore the $\underline{v}^{ab}$'s can be divided into two parts, $\underline{\tilde{v}}^{ab}$ and $\underline{M}^{ab}$ where $\Sigma_a\underline{\tilde{v}}^{aa}=0$ and $\underline{M}^{ab}$ is built up from the previously mentioned constants of motions, $\mathcal{O}^a$. Then as we shall see, at the stable fixed points of Eq. (5.6) the $\underline{\tilde{v}}^{ab}$'s can be written as

$$(\underline{\tilde{v}}^{ab})_{\rm fp}=\frac{1}{f}\begin{pmatrix}\underline{L}^{ab} & 0\\ 0 & 0\end{pmatrix}, \tag{5.7}$$

where the $\underline{L}^{ab}$'s satisfy the standard SU(N) Lie algebra,

$$[\underline{L}^{ab},\underline{L}^{cd}]=\delta^{ad}\underline{L}^{cb}-\delta^{cb}\underline{L}^{ad}, \tag{5.8}$$

and are unitary equivalent to the defining representation: $L^{ab}_{nn'}\sim\delta^a_n,\delta^b_n-(1/f)\,\delta^{ab}\delta_{nn'}$. This statement is also demonstrated in Fig. 23, where the scaling of the ''algebra coefficient'' $\alpha=\Sigma_{a,b,c,d}\|f^2[\underline{\tilde{v}}^{ab},\underline{\tilde{v}}^{cd}]-f\delta^{ad}\underline{\tilde{v}}^{cb}+f\delta^{cb}\underline{\tilde{v}}^{ad}\|$ is shown, measuring how well the fixed-point algebra (5.8) is satisfied. As one can see in Fig. 23 for $D\ll T_K$ the algebra coefficient α vanishes and, therefore, in an appropriate basis, the $\underline{\tilde{v}}^{ab}$'s really simplify to the form in Eq. (5.7).

Equation (5.7) means that *at the fixed point* $\underline{\tilde{v}}^{ab}$ is given by Eq. (5.7), and apart from some potential scattering term the fixed-point effective interaction can be written as

$$H_{\rm eff}=V_0\sum_{\substack{a,b\\ \epsilon,\epsilon',m}}\chi^+_a c^+_{\epsilon bm}c_{\epsilon' am}\chi_b\,, \tag{5.9}$$

which is the same as the interaction term in Eq. (2.1). Note that while the initial model was very asymmetrical in the orbital space, at the fixed point *only N conduction electron angular momentum channels* are coupled to the NLS, and the fixed-point effective Hamiltonian already shows an additional SU(N) symmetry in the orbital sector as well. These statements are not true away from the fixed point, where various kinds of irrelevant operators couple the NLS to the electrons, and coupling to the other orbital channels is also relevant. The effective Hamiltonian is completely symmetrical in the NLS site index, which means that, e.g., the amplitude of assisted tunneling from site 1 to 6 in Fig. 23 is the same as the nearest-neighbor-assisted tunneling amplitude from site 1 to 2, despite their different geometrical positions.

As will become obvious in Sec. V B, the analysis above is based on the possibility of a systematic N/f expansion. Therefore, it is strictly valid in the $f>N$ case. However, one has several arguments that the effective Hamiltonian equation (5.9) is also adequate for the $N\leqslant f$ cases. First of all, in the case $N=2$ corresponding to the simpler case of multichannel Kondo model, it is well known that for $f=1$ and $f=2$ the spin anisotropy of the couplings is *irrelevant* around the fixed point,[1,26] which has the same SU(2) structure as Eq. (5.7). Furthermore, for $f=1$ but *arbitrary N* one can easily prove following similar lines as Nozières and Blandin[1] that the isotropic fixed point [Eq. (5.9)] is stable against spin (orbital) anisotropy. These observations together with our results for the $f>N$ case make it highly improbable that for $2\leqslant f\leqslant N$ the NLS model would have a stable fixed point different from the one discussed above.

B. Stability analysis of the SU(N)×SU(f) fixed point of the NLS model in the large f limit

The statement that $\underline{\tilde{v}}^{ab}$ is a fixed point of Eq. (5.6) is trivial. However, we also want to prove the stability of this fixed point analytically, and find the irrelevant operators (determining the low-energy behavior of the model) around it. To this end we write the deviations from the fixed point in the form

$$\underline{\delta v}^{ab}=\begin{pmatrix}\underline{\varrho}^{ab} & \underline{t}^{ba}\\ (\underline{t}^{ab})^+ & \underline{\mu}^{ab}\end{pmatrix}, \tag{5.10}$$

where the couplings $\underline{\varrho}^{ab}$, $\underline{t}^{ab}$, and $\underline{\mu}^{ab}$ are $N\times N$, $N\times\infty$, and $\infty\times\infty$ matrices, respectively. Substituting this expression into Eq. (5.6), one obtains the following linearized decoupled scaling equations:

$$\frac{d\underline{\mu}^{ab}}{dx}=\frac{1}{f}(\delta^{ab}\underline{\mu}^{dd}-N\underline{\mu}^{ab}), \tag{5.11}$$

$$\begin{aligned}\frac{d\underline{\varrho}^{ab}}{dx}=&-\frac{1}{f}([\underline{L}^{ad},\underline{\varrho}^{db}]+[\underline{\varrho}^{ad},\underline{L}^{db}])+\frac{1}{2f}\{2\delta^{ab}\underline{\varrho}^{dd}\\&+2\underline{L}^{cd}\mathrm{tr}\{\underline{\varrho}^{ac}\underline{L}^{db}+\underline{L}^{ac}\underline{\varrho}^{db}\}-2N\underline{\varrho}^{ab}\\&-\underline{L}^{ac}\mathrm{tr}\{\underline{\varrho}^{cd}\underline{L}^{db}+\underline{L}^{cd}\underline{\varrho}^{db}\}\\&-\mathrm{tr}\{\underline{\varrho}^{ac}\underline{L}^{cd}+\underline{L}^{ac}\underline{\varrho}^{cd}\}\underline{L}^{db}\},\end{aligned} \tag{5.12}$$

$$\frac{dt^{ab}}{dx}=-\frac{1}{f}(\underline{L}^{ad}t^{db}-\underline{L}^{db}t^{ad})+\frac{1}{f}(\delta^{ab}t^{dd}-Nt^{ab}). \tag{5.13}$$

The solution of Eq. (5.11) is trivial, since the operator $\underline{\mu}^{ab}$ can be decomposed as $\underline{\mu}^{ab}=[\underline{\mu}^{ab}-\delta^{ab}(1/N)\underline{\mu}^{cc}]+[\delta^{ab}(1/N)\underline{\mu}^{cc}]$, where the first operator scales like $T^{\lambda}\sim e^{-x\lambda}$ with a dimension $\lambda=\lambda_{\mathrm{sl}}=N/f$, while the second is marginal with $\lambda=0$. The detailed analysis of the other two equations is much more complicated, but still one can find their exact solutions due to the simple structure of the $\underline{L}^{ab}$'s Here we only briefly discuss the results of this analysis.

It turns out that Eqs. (5.12) and (5.13) have an infinite number of zero modes that can be divided into two distinct classes. The first type corresponds to potential scattering off the NLS, and can be written as

$$\underline{\delta v}^{ab}_{\mathrm{pot}}=\delta^{ab}\underline{\delta v}, \tag{5.14}$$

where δv denotes an arbitrary $\infty\times\infty$ Hermitian matrix. The rest of the zero modes can be identified with the generators $\delta v^{ab}_{\mathrm{gen}}$ of the unitary transformations of the SU(N) Lie algebra, Eq. (5.8),

$$\underline{\delta v}^{ab}_{\mathrm{gen}}=\begin{pmatrix}\underline{\varrho}^{ab}_{\mathrm{gen}} & \underline{t}^{ab}_{\mathrm{gen}}\\ (\underline{t}^{ba})^{+}_{\mathrm{gen}} & 0\end{pmatrix}. \tag{5.15}$$

More precisely, the generators $\underline{\varrho}^{ab}_{\mathrm{gen}}$ and $\underline{t}^{ab}_{\mathrm{gen}}$ can be shown to satisfy in first order the equations

$$\begin{aligned}\underline{L}^{ab}\underline{t}^{cd}_{\mathrm{gen}}-\underline{L}^{cd}\underline{t}^{ab}_{\mathrm{gen}}&=\delta^{ad}\underline{t}^{cb}_{\mathrm{gen}}-\delta^{cb}\underline{t}^{ad}_{\mathrm{gen}},\\ [\underline{L}^{ab},\underline{\varrho}^{cd}_{\mathrm{gen}}]+[\underline{L}^{cd},\underline{\varrho}^{ab}_{\mathrm{gen}}]&=\delta^{ad}\underline{\varrho}^{cb}_{\mathrm{gen}}-\delta^{cb}\underline{\varrho}^{ad}_{\mathrm{gen}},\end{aligned} \tag{5.16}$$

from which it follows that the operators $\tilde{\underline{L}}^{ab}:=\underline{L}^{ab}+\underline{\delta v}^{ab}_{\mathrm{gen}}$ satisfy the same Lie algebra as the original $\underline{L}^{ab}$'s:

$$[\tilde{\underline{L}}^{ab},\tilde{\underline{L}}^{cd}]=\delta^{ad}\tilde{\underline{L}}^{cb}-\delta^{cb}\tilde{\underline{L}}^{ad}. \tag{5.17}$$

The $\underline{\varrho}^{ab}_{\mathrm{gen}}$'s turn out to be the generators of the unitary transformations in the N dimensional electronic subspace where the Lie-algebra Eq. (5.8) is realized, while the $\underline{t}^{ab}$'s correspond to the rotations of this N-dimensional subspace.

All the other eigenoperators around the fixed point can be shown to be irrelevant. Very surprisingly, at least in the large-f limit, the leading irrelevant operators are quite different from the leading irrelevant operator of the SU(N) $\times$SU(f) model (5.9), both in their structure and in their scaling dimension. They are living in the sector $\underline{t}^{ab}$, and they can be written

$$\underline{\delta v}^{ab}_{1}=\begin{pmatrix}0 & \underline{C}^{ab}\\ (\underline{C}^{ba})^{+} & 0\end{pmatrix}, \tag{5.18}$$

where the C^{ab}_{cm}'s satisfy $\Sigma_a C^{aa}_{cm}=0$ and $\Sigma_b(C^{ab}_{cm}-C^{cb}_{am})=0$ with $a,b,c=1,...,N$ and $n=N+1$, $N+2,\ldots,\infty$. These operators have a dimension

$$\lambda_1=\frac{N-1}{f}+\vartheta\left(\frac{N^2}{f^2}\right). \tag{5.19}$$

We remark at this point that the operators (5.18) do *not exist* in the two-level-system model, which is therefore completely equivalent to the corresponding SU(2)$\times$SU(f) model.[17] As we shall see, these operators do not give a contribution to physical quantities like the resistivity or the impurity susceptibility, but they influence the thermodynamic behavior of the model. We stress at this point, that their existence is strictly proved in the $f\to\infty$ limit. They are very probably present even in the $N<f$ case but it is an open question if they survive in the $N\leqslant f$ limit.

The impurity resistivity will be shown to be dominated by the subleading operators

$$\underline{\delta v}^{ab}_{\mathrm{sl}}\sim\begin{pmatrix}\underline{Q}^{ab} & 0\\ 0 & \underline{S}^{ab}\end{pmatrix}, \tag{5.20}$$

where the matrices $\underline{Q}^{ab}$ and $\underline{S}^{ab}$ satisfy $\underline{Q}^{aa}=\underline{S}^{aa}=0$ and $Q^{ab}_{dc}=Q^{ab}_{dc}$. These operators have a dimension

$$\lambda_{\mathrm{sl}}=\frac{N}{f}+\vartheta\left(\frac{N^2}{f^2}\right), \tag{5.21}$$

and operator (5.9) considered in the SU(N)$\times$SU(f) model is also one of them. Furthermore, one has other even more irrelevant operators in the $\underline{t}$ sector of δv with a dimension $\lambda_{\mathrm{ssl}}=(N+1)/f$ which give a subleading contribution to the physical quantities calculated.

In the previous considerations we did not take into account the presence of the splitting Δ^{ab} of the NLS. As we discussed already, this splitting results in the appearance of another low-energy scale T^*. Below this the NLS cannot jump freely between its N different positions. Since usually the ground state of the *NLS* is nondegenerate in most cases, a Fermi-liquid state develops. In other words, the non-Fermi-liquid SU(N)$\times$SU(f) fixed point is unstable with respect to the splitting that usually drives the system toward a Fermi-liquid ground state.

It has been argued very recently[27] that in special cases, due to some dynamical Jahn-Teller effect, e.g., the hopping amplitude Δ^{ab} might pick up and additional Berry phase, which could then result in a degenerate ground state with degeneracy N'. Then the effective Hamiltonian at very low temperatures would be, of course, an SU(N')$\times$SU(f) exchange model, and in the region $T\ll T^*$ all our previous considerations hold with the replacement of N by N'. Unfortunately, this Berry phase scenario will very probably not occur and therefore the non-Fermi-liquid behavior can most

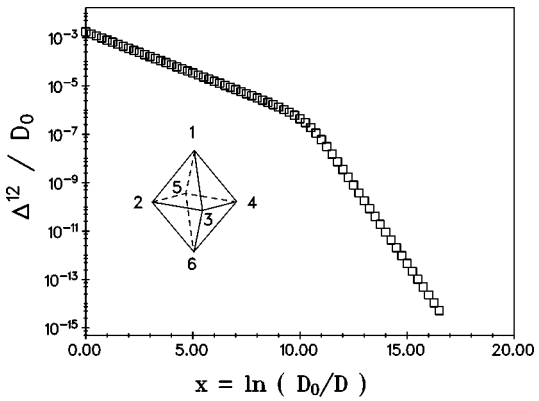

FIG. 24. Scaling of the dimensionless hopping amplitude, Δ^{12}/D_0 for the same six-state system as in Fig. 23. Inset: numbering of the sites of the six-state system.

probably be observed only in the restricted temperature (energy) range $T^* < \max\{T,\omega\} < T_K$, i.e., when the freezing temperature is small enough.

Therefore, it is very important to determine the realistic values of the freezing temperature. We estimated the freezing temperature by solving the scaling equations (5.5) and (5.6) numerically for the same symmetrical six-level system as in Fig. 23. In this case the diagonal matrix elements Δ^{aa} vanish by symmetry. As one can see from Fig. 24, for a realistic NLS the renormalization of the hoppings Δ^{ab} is huge, and the situation $T^* < \max\{T,\omega\} < T_K$ can be reached quite easily. We note at this point that in our Hamiltonian we also neglected the contribution of two-electron scattering around the fixed point, which might be also relevant in the immediate neighborhood of the fixed point.[27] However, these have a very small amplitude and they are scaled downwards in the first part of the scaling, $D > T_K$. Therefore, most probably their effect can be neglected compared to that of the splitting Δ^{ab}, which provides the dominant mechanism to drive the system finally to a Fermi-liquid state.[28]

C. Scaling of the physical quantities of the NLS model in the large-*f* limit

Now we turn to the calculation of the physical quantities. In this subsection we shall determine different thermodynamic quantities and the conduction electrons' scattering rate $1/\tau$, which is directly proportional to the impurity contribution to the electrical resistivity $R_{\rm imp}(T)$.

To calculate a general physical quantity, one should also calculate the renormalization coefficient A in Eq. (5.3), which is quite a nontrivial task away from the fixed point. However, one can easily convince himself that in the free-energy corrections in Fig. 25 and the electronic self-energy corrections in Fig. 22(c) the factors A and A^{-1} cancel exactly, and therefore that these are *scale invariant*, and can be calculated by solving solely the scaling equations (5.5) and (5.6).

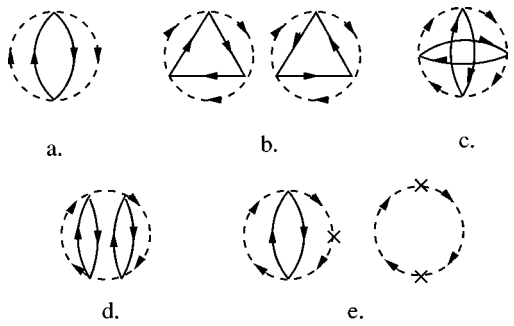

FIG. 25. Diagrams generating the $1/f^2$ corrections to the free energy. The crosses denote the counterterm.

For the sake of simplicity let us assume first that the highest low-energy scale is given by the temperature. To calculate a physical quantity at a temperature T we apply a renormalization-group transformation (5.3) with $D = D_0$ and $D' = T$. Then in the new Hamiltonian all the logarithmic terms vanish since $\ln(D'/T) = 0$, and the different physical quantities are exclusively given by the *nonlogarithmic contributions* of the corresponding diagrams. For a scale-invariant quantity like the free energy, e.g., this implies that

$$F_{\rm imp}(D_0, T, \underline{v}_0^{ab}, \Delta_0^{ab}) = F_{\rm imp}\left[T, T, \underline{v}^{ab}\left(\ln\frac{D_0}{T}\right),\ \Delta^{ab}\left(\ln\frac{D_0}{T}\right)\right], \qquad (5.22)$$

where on the right-hand side no logarithmic corrections appear, but renormalized couplings have to be used.

Therefore, in order to calculate the scaling behavior of the thermodynamic quantities, our task is to determine the nonlogarithmic parts of the different free energy diagrams. Since the fixed point couplings $\underline{v}_{\rm fp}^{ab}$ are proportional to $1/f$ up to $1/f^2$ order only the diagrams in Figs. 25(a)–25(d) contribute. However, these diagrams contain divergent contributions originating from the finite part of the self-energy diagram in Fig. 22(b). These spurious divergences can be handled by a standard renormalization procedure,[29] by adding the following counterterm to the Hamiltonian:

$$H_{\rm count} = f\ 2D\ \ln 2 \chi_a^+ \chi_c {\rm tr}\{\underline{v}^{ab}\underline{v}^{bc}\}. \qquad (5.23)$$

This counterterm can also be interpreted as a renormalization of the bare parameters of the model, which should be used in Eq. (5.3) as the initial conditions. Then the counterterm contributions in Fig. 25(e) cancel all the spurious divergences, and after a tedious calculation one obtains, for the nonlogarithmic part of the free energy,

$$F_{\rm imp} = -T\left[\ln N + \frac{2\pi^2 f}{3N}({\rm tr}\{\underline{v}^{ab}\underline{v}^{bc}\underline{v}^{ca} - \underline{v}^{ca}\underline{v}^{bc}\underline{v}^{ab}\}) - \frac{f^2\pi^2}{2N}({\rm tr}\{\underline{v}^{ab}\underline{v}^{cd}\}{\rm tr}\{\underline{v}^{bc}\underline{v}^{da}\} - {\rm tr}\{\underline{v}^{ab}\underline{v}^{bc}\}{\rm tr}\{\underline{v}^{cd}\underline{v}^{da}\}) + \cdots\right]. \qquad (5.24)$$

Note that diagram (a) in Fig. 25 is proportional to T^2/D, and it does not give a contribution in the scaling limit.

Substituting the fixed point couplings Eq. (5.7) into Eq. (5.24) the fixed-point entropy can be calculated as

$$S_{\rm imp}=\frac{\partial F_{\rm imp}}{\partial T}\approx \ln N-\frac{N^2-1}{f^2}\,\frac{\pi^2}{6}, \tag{5.25}$$

which is just the expanded version of Eq. (3.18). Note that Eq. (5.25) gives the NLS contribution to the entropy only in the region $T^*\ll T\ll T_K$. Below T^* the motion of the NLS is usually frozen out and the impurity entropy tends to zero, corresponding to a Fermi-liquid state.

The scaling of the free energy in the region $T^*\ll T\ll T_K$ can be determined by expanding the $\underline{v}^{ab}$'s around their fixed-point values like Eq. (5.10), and substituting them into Eq. (5.24). It turns out that similarly to the multichannel Kondo and the two-level system case[16,17] only the second order terms in $\underline{\delta v}^{ab}$ contribute, and therefore in the temperature range $T^*\ll T\ll T_K$ in leading order the free energy and the specific heat scale as

$$F_{\rm imp}\sim T\left(\frac{T}{T_K}\right)^{2\lambda_1}\sim T^{[2(N-1)/f]+1}, \tag{5.26}$$

$$c_{\rm imp}\sim\left(\frac{T}{T_K}\right)^{2(N-1)/f}. \tag{5.27}$$

Below T^* the free energy generally shows a Fermi-liquid behavior. This scaling behavior does not agree with the one obtained in the Bethe ansatz (BA) solution of the exchange model. However, we have to remark at this point that, according to our estimations, the amplitude of the subleading operators in $\underline{\delta v}^{ab}$ is *larger* than that of the leading irrelevant operators. Therefore, one expects that there is a substantial energy region where the subleading operators dominate, and eventually it is also possible that they dominate the scaling of the free energy in the whole region $T^*\ll T\ll T_K$. Then the exponent λ_1 in Eq. (5.26) should be replaced by $\lambda_{\rm sl}$, and one obtains a scaling $c_{\rm imp}\sim T^{2N/f}$ which is in $1/f$ order completely identical to the Bethe ansatz and conformal field theory results for the SU(N)×SU(f) model.

One can also easily determine the scaling of the splitting susceptibility $\chi_\Delta=\partial^2 F_{\rm imp}/\partial\Delta^2$ at $T=0$ for small Δ's, where now Δ denotes the characteristic value of the splittings Δ^{ab}. Investigation of the free-energy diagrams (Fig. 25) shows that the ''splitting magnetization'' $M_\Delta=\partial F_{\rm imp}/\partial\Delta$ should be of the form

$$M_\Delta=m\left(\frac{\Delta}{D},\underline{v}^{ab}\right). \tag{5.28}$$

The important point is that Δ is not scale invariant, but rather behaves as

$$\Delta'=Z_\Delta\left(\frac{D_0}{D},\underline{v}^{ab}\right)\Delta, \tag{5.29}$$

where the factor Z_Δ should be determined by integrating Eq. (5.5). As a consequence, M_Δ is *not scale invariant* either, and has to be rescaled under the renormalization-group transformation by the factor Z_Δ. Therefore, applying the renormalization-group transformation to Eq. (5.28) with $D'=\Delta^*=T^*$, we obtain.

$$M_\Delta=Z_\Delta\left(\frac{D_0}{\Delta^*},\underline{v}^{ab}\right)\times m(1,\underline{v}^{ab}_{\rm fp}), \tag{5.30}$$

where we assumed that $\Delta^*\ll T_K$ and thus the scaled couplings $\underline{v}^{ab}(D')$ can be replaced by their fixed-point values. Since $m(1,\underline{v}^{ab}_{\rm fp})$ is just a constant, the scaling of M_Δ is the same as that of the factor $Z_\Delta(D_0/\Delta^*,\underline{v}^{ab})$. For very small Δ's, the scaling of Z_Δ can easily be determined from the fixed-point form of the scaling equation (5.5)

$$\frac{d\Delta^{ab}}{dx}=-\frac{N}{f}\Delta^{ab}, \tag{5.31}$$

and one obtains, in leading order in $1/f$,

$$M_\Delta\sim Z_\Delta\left(\frac{D_0}{\Delta^*}\right)\sim\left(\frac{\Delta^*}{T_K}\right)^{N/f}\approx\left(\frac{\Delta}{T_K}\right)^{N/f}, \tag{5.32}$$

in agreement with Eq. (3.29) and the conformal field theory results.[30] In higher order in $1/f$, one also has to take into account the renormalization of the splitting in Eq. (5.32), $\Delta^*\sim\Delta^{1/(1-\lambda_{\rm sl})}$, and one obtains with $\lambda_{\rm sl}=[N/(N+f)]\approx(N/f)-(N^2/f^2)$

$$M_\Delta\sim\Delta^{\lambda_{\rm sl}/(1-\lambda_{\rm sl})}\sim\Delta^{N/f}, \tag{5.33}$$

which is the exact result.[15,30]

Finally, we discuss the scaling of the electronic scattering rate, which we determine from the imaginary part of the electronic self-energy in Fig. 22(c). By assuming a finite impurity concentration n_i and averaging over the position of the impurities and the orientation of the incoming electrons, for the average scattering rate we obtain

$$\left\langle\frac{1}{\tau}\right\rangle=2\pi n_i(2D_0)\,\frac{1}{N}\,{\rm tr}\{\underline{v}^{ab}\underline{v}^{ba}\}. \tag{5.34}$$

Note that the factor D_0 arises from the inverse density of states ϱ_0^{-1} and is invariant under scaling. Substituting into this equation $\underline{v}^{ab}=\underline{v}^{ab}_{\rm fp}+\underline{\delta v}^{ab}$, we see immediately that the leading irrelevant operators do not give a contribution to the electronic scattering rate, which is dominated by subleading operators and scales like

$$\frac{1}{\tau}\sim T^{\lambda_{\rm sl}}\sim T^{N/f}\quad(\omega=0),$$

$$\frac{1}{\tau}\sim\omega^{N/f}\quad(T=0). \tag{5.35}$$

In higher orders this result should be replaced by $1/\tau\sim T^{N/(f+N)}$ and $1/\tau\sim\omega^{N/(f+N)}$.

D. Discussion of the possible physical realizations of the NLS model

The simplest possible realization of the SU(N)×SU(f) model is given by substitutional impurities in metals. These impurities may form tunneling centers[31,32] which then interact with the conduction electrons' band. An example of such

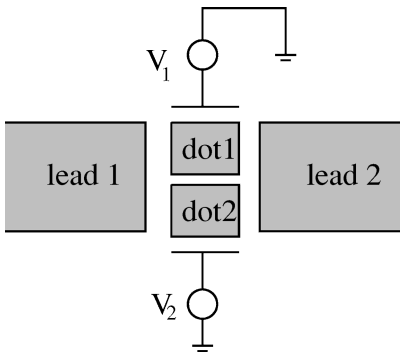

FIG. 26. A mesoscopic double-dot system, a candidate for the SU(3)×SU(2) model.

a system is given by $Pb_{1-x}Ge_xTe$.[32] The alloy PbTe is a narrow-gap semiconductor, but usually because of some intrinsic impurities it becomes metallic at low temperatures. Since the Ge^{2+} ions are smaller than the Pb^{2+} ions, and they are also attracted by their nearest neighbor Te^{2-} ions, they form eight-state systems, and according to the our discussions in Sec. V A they would be good candidates for the SU(8)×SU(2) model.

However, while an unambiguous logarithmic anomaly has been observed in the resistivity of these materials,[32] no non-Fermi-liquid behavior has been detected. There may be several reasons for that. According to the results of the BA calculations in the case $N>f$ the non-Fermi-liquid corrections are *subleading*, and the physical quantities have in leading order a Fermi-liquid-like behavior. The subleading low-temperature behavior of these alloys has never been analyzed, and the original measurements do not seem to be accurate enough to extract such a subleading behavior from them. We are not aware of any measurement of other physical quantities like the specific heat in the interesting concentration domain. Furthermore, PbTe has very complicated properties: it has a soft-phonon mode that drives the system through a ferroelectric phase transition as a function of the Ge concentration, and there is a strong spin-orbit scattering in it, which probably spoils the SU(2) symmetry of the electron spins as well. Moreover, the measurements have been carried out at relatively large Ge concentrations, where the interaction of the NLS's can no lonber be neglected.

It seems to be that in order to observe non-Fermi-liquid scaling, much more accurate measurements should be carried out at even lower temperatures for *several* physical quantities and *lower* Ge concentrations. One could also try to find a better candidate. Since in the case of PbTe the formation of the NLS's is induced by the ionic attractions, we think that experimentalists should search among multicomponent metals, where some interstitials can be solved in the material.

Similarly to the case of the two-channel Kondo model,[33] another possible realization of the SU(N)×SU(f) model could be possible by means of nanotechnologies. In Fig. 26, we show a double-dot geometry which is a candidate for the realization of the SU(3)×SU(2) model. In the leads the electrons can be described as free particles:

$$H_{\text{leads}}=\sum_{\alpha=l1,l2}\sum_{\epsilon\sigma}\epsilon c^{+}_{\epsilon\alpha\sigma}c_{\epsilon\alpha\sigma}, \tag{5.36}$$

where $\alpha=l1,l2$ refers to the two leads, and $\sigma=\pm$ is the electron spin.

The Hamiltonian of the dots can be written as[34]

$$H_{\text{dots}}=\sum_{\alpha=d1,d2}\sum_{\epsilon\sigma}\epsilon c^{+}_{\epsilon\alpha\sigma}c_{\epsilon\alpha\sigma}+\frac{(Q_1-V_1C_1)^2}{2C_{\Sigma,1}}+\frac{(Q_2-V_2C_2)^2}{2C_{\Sigma,2}}+\frac{Q_1Q_2}{C_{12}}, \tag{5.37}$$

where $\alpha=d1,d2$ is the index of the two dots, Q_1 and Q_2 are the charges of them, V_1 and V_2 denote the applied gate voltages in the figure, and the C's denote different capacitances of the system.[35] With a suitable choice of the gate voltages one can achieve that the ground state of the dots becomes three times degenerate corresponding to the states $\beta:=(Q_1,Q_2)=(0,0)$, $(0,e)$, and $(e,0)$. Then the tunneling processes among the leads and dots result in simultaneous flips in the electrons orbital quantum number $\alpha=\{l1,l2,d1,d2\}$ and the charge variables β which now take over the role of the orbital index of the NLS. Since the tunneling is diagonal in the electrons' spin, we have an additional SU(2) degeneracy in the spin of the electrons. Therefore this system is a good candidate for the realization of the SU(3)×SU(2) model, where the SU(3) fixed point symmetry corresponds to the three times degenerate ground states of the dots.

VI. CONCLUSIONS

We have studied the multichannel Coqblin-Schrieffer model (MCCS) and its relation to the N-level system (NLS) model. The properties of the MCCS model depend on both the spin and flavor symmetries, SU(N) and SU(f), as well as on the *spin* of the impurity.

We have performed both analytical and numerical studies of the model. As with the multichannel Kondo model, there are three different classes of fixed points depending on the spin of the impurity, μ. The underscreened and completely screened fixed points ($\mu>f$ and $\mu=f$, respectively) have qualitatively similar behaviors to the analogous multichannel counterparts ($N=2$).

There are overscreened fixed points. They display non-Fermi-liquid behavior. They have associated anomalous residual entropy and anomalous exponents in the low-temperature expansion of quantities like the specific heat and the magnetic susceptibility.

For an impurity with spin in the fundamental representation of SU(N), the residual entropy, $\mathcal{S}^i$, is only a function of $N+f$ and $|\ln(N/f)|$. Hence there are different fixed points with the same value of $\mathcal{S}^i$. The exception corresponds to $N=f$, which yields the largest value of the residual entropy for fixed $N+f$.

The low-temperature thermodynamics are determined by the value of the ratio $\gamma=f/N$ alone, for any $\mu<f$. When $f\neq N$, we have

$$\frac{C_V^i}{T},\quad \chi^i\propto\text{const.}+\left(\frac{T}{T_K}\right)^{(1-\gamma)/(1+\gamma)}, \tag{6.1}$$

which diverge for $\gamma>1$, but remain finite for $\gamma<1$. When $N=f$, the power is replaced by a logarithm, as in the two-

channel Kondo model. The constant terms in Eq. (6.1) are always present and when they are they are the dominant contributions in the completely screened case, $\mu = f$, and when $f < N$. The Wilson ratio in such cases is given by

$$R = \frac{N(N+f)}{N^2-1}.$$

Channel anisotropy is a relevant perturbation. As the channel symmetry is reduced from SU(f) to SU(f'), the entropy is quenched since $N+f$ decreases and $|\ln(N/f)|$ increases. Likewise, a system with channel anisotropy might behave like a $f > N$ system at intermediate temperatures and flow at low-T to a $f < N$ system.

Then we turned to the comparison of the MCCS model to the N-level system model describing a heavy particle tunneling between N different positions and interacting with the conduction electrons. We have shown that the low-energy fixed point of the NLS model is just the SU(N)$\times$SU(f) MCCS model. Performing a large $1/f$ study of the NLS model, we have analyzed the operator content of this low-energy fixed point, and the scaling properties of different physical quantities in the $N < f$ limit. We have shown in this limit that while the operator content of the NLS model is different from that of the MCCS model, apart from some subtle differences, the low-energy properties of the two models are the same. In particular, comparison with the exact results obtained in the first part of the paper and with the NCA calculations[15] show that the susceptibility, the residual entropy, and the resistivity of the two models behave in the same way, and for reasonable physical parameters even the scaling of the specific heat is properly described by the MCCS model.

Finally, we discussed some possible physical realizations of the SU(N)$\times$SU(f) models. First we discussed the case of tunneling interstitials in multicomponent metals such as $Pb_{1-x}Ge_xTe$ compounds. We pointed out that the low concentration of interstitials is essential to avoid strong interimpurity interactions and keep the diagonal elements of the self-energy Δ^{ab} small. Secondly, we suggested a double quantum-dot structure that could give an ideal realization for the SU(3)$\times$SU(2) model.

ACKNOWLEDGMENTS

During the course of this investigation we learned of parallel work by A. Georges, O. Parcollet, G. Kotliar, and A. Sengupta, using conformal field theory and a large-N approach to study the same model. There was perfect agreement whenever comparison could be made. We are most grateful to the above authors for many useful and enlightening discussions and for sharing their results prior to publication. Part of the work was carried out while N. A. was visiting the Physique Theorique group at the ENS. It is a pleasure to thank the members of the group for their warm hospitality. G. Z. would like to acknowledge useful discussions with D. L. Cox, K. Vladár, A. Zawadowski, and A. Moustakas. He would like to thank the Magyary Zoltán Foundation and the Institut Laue-Langevin (Grenoble) for its hospitality, where part of the present work was done. A. J. would like to acknowledge useful discussions with R. Bulla, P. Coleman, F. H. L. Essler, A. Hewson, A. F. Ho, A. Lopez, P. Nozières, R. Ramazashvili, and A. Tsvelik. The numerical calculations were carried out using the computing facilities of Theoretical Physics, University of Oxford. N. A. is grateful to C. Destri and D. Braak for sharing their insights during the course of many illuminating discussions, and to A. Ruckenstein for a careful reading of the manuscript. This research was supported by EPSRC Grant No. GR/K97783, Hungarian Grant Nos. OTKA F016604 and OTKA 7283/93, and the U.S.-Hungarian Joint Fund No. 587.

*Present address: Institut Laue-Langevin, Grenoble, France.

[1] P. Nozières and A. Blandin, J. Phys. (Paris) **41**, 193 (1980).
[2] A. Zawadowski, Phys. Rev. Lett. **45**, 211 (1980); K. Vladár and A. Zawadowski, Phys. Rev. B **28**, 1564 (1983); **28**, 1582 (1983); **28**, 1596 (1983); A. Zawadowski and K. Vladár, in *Quantum Tunneling in Condensed Media*, edited by Yu. Kagan and A. J. Leggett (North-Holland, Amsterdam, 1992).
[3] D. L. Cox, Phys. Rev. Lett. **59**, 1240 (1987).
[4] D. L. Cox and A. Zawadowski, cond-mat/9704103 (unpublished).
[5] G. Zaránd, Phys. Rev. Lett. **77**, 3609 (1996); N. Andrei (unpublished).
[6] N. Andrei and C. Destri, Phys. Rev. Lett. **52**, 364 (1984).
[7] C. Destri (unpublished).
[8] N. Andrei, in *Integrable Models in Condensed Matter Physics*, edited by S. Lundquist, G. Morandi, and Yu Lu, Series on Modern Condensed Matter Physics Vol. 6 (World Scientific, Singapore, 1992), pp. 458–551.
[9] P. Zinn-Justin and N. Andrei, cond-mat/9801158 (unpublished).
[10] S. Okubo, J. Math. Phys. **18**, 2382 (1977).
[11] H. F. Jones, *Groups, Representations and Physics* (Institute of Physics and Physical Society, Bristol, 1990).
[12] N. Andrei, K. Furuya, and J. H. Lowenstein, Rev. Mod. Phys. **51**, 331 (1983).
[13] A. Tsvelik and P. Wiegman, Adv. Phys. **32**, 453 (1983).
[14] A. M. Tsvelik, Zh. Eksp. Teor. Fiz. **93**, 1329 (1987) [Sov. Phys. JETP **66**, 754 (1987)].
[15] D. L. Cox and A. E. Ruckenstein, Phys. Rev. Lett. **71**, 1613 (1993).
[16] J. Gan, N. Andrei, and P. Coleman, Phys. Rev. Lett. **70**, 686 (1993).
[17] G. Zaránd, Phys. Rev. B **51**, 273 (1995); G. Zaránd and K. Vladár, Phys. Rev. Lett. **76**, 2133 (1996).
[18] N. Andrei and A. Jerez, Phys. Rev. Lett. **74**, 4507 (1995).
[19] N. Andrei and H. Johannesson, Phys. Lett. **104A**, 370 (1984).
[20] V. T. Rajan, Phys. Rev. Lett. **51**, 308 (1985).
[21] W. H. Press *et al.*, *Numerical Recipes in Fortran* (Cambridge University Press, Cambridge 1992).
[22] H.-U. Desgranges, J. Phys. C **18**, 5481 (1983).
[23] J. Kondo, Physica B & C **84**, 40 (1976).
[24] A. A. Abrikosov, Physics (Long Island City, NY) **2**, 5 (1965).
[25] A. Muramatsu and F. Guinea, Phys. Rev. Lett. **57**, 2337 (1986).
[26] H. B. Pang and D. L. Cox, Phys. Rev. B **44**, 9454 (1991).
[27] A. L. Moustakas and D. S. Fisher, Phys. Rev. B **53**, 4300 (1996); *ibid.* **55**, 6832 (1997).
[28] A. Zawadowski *et al.* (unpublished).

[29] For a general introduction, see, e.g., C. Itzykson and J. B. Zuber, *Quantum Field Theory*, McGraw-Hill International Editions, Singapore, 1980.
[30] I. Affleck and A. W. W. Ludwig, Nucl. Phys. B **428**, 545 (1994).
[31] M. Tornow *et al.*, Physica B **194–196**, 1063 (1994).
[32] S. Katayama, S. Maekawa, and H. Fukuyama, J. Phys. Soc. Jpn. **56**, 697 (1987).
[33] A. Furusaki and K. A. Matveev, Phys. Rev. B **52**, 16 676 (1995).
[34] M. Devoret, in *Les Houches Summer School on Mesoscopic Quantum Physics*, edited by E. Akkermans *et al.* (North-Holland, Amsterdam, 1995).
[35] D. V. Averin and K. K. Likharev, in *Mesoscopic Phenomena in Solids*, edited by B. L. Altschuler *et al.* (North-Holland, Amsterdam, 1991).